PRODUCTION OF HADRONS IN CHARGED-CURRENT NEUTRINO AND ANTINEUTRINO REACTIONS

Norbert Schmitz

Max-Planck-Institut für Physik und Astrophysik
München, Germany

A.) Introduction

Recent results on hadron production in charged-current (CC) neutrino and antineutrino reactions

$$\text{(1)} \qquad \begin{array}{ll} \nu + N \to \mu^- + \text{hadrons} & \text{, i.e. } W^+ + N \to \text{hadrons} \\ \bar{\nu} + N \to \mu^+ + \text{hadrons} & \text{, i.e. } W^- + N \to \text{hadrons} \end{array}$$

come from the bubble chamber experiments listed in Table 1. Papers on the subject which have appeared in 1980 and 1981 from these experiments are given as references [1-44]. Four bubble chambers have contributed, namely the 15' chamber at Fermilab, the Big European Bubble Chamber BEBC and Gargamelle (GGM) at CERN, and the heavy-liquid chamber SKAT at Serpukhov. Both neutrino and antineutrino beams have been used. Reactions have been investigated on protons p (hydrogen or deuterium targets), neutrons n (deuterium targets) and isoscalar nucleons N (heavy liquid targets). In particular, new results have been obtained on νn and $\bar{\nu} n$ scattering from the two experiments with deuterium in the 15' chamber and in BEBC, respectively. Deuterium as a target has of course the advantage that reactions on protons and on neutrons can be studied at the same time. In the antineutrino experiments the ν contamination in the $\bar{\nu}$ beams has sometimes been used to investigate also neutrino reactions whereas the $\bar{\nu}$ contamination in ν beams is rather small. The situation of neutrinoproduction of hadrons as of one year ago has been reviewed by Saitta at Erice [45].

Table 1: Experiments with recent (1980,1981) results on hadronic final states.

Bubble chamber, Liquid	Beam	Collaboration	References
15' H_2	$\bar{\nu}$ (ν) WB	Argonne, Carnegie-Mellon, Purdue	[1-5]
15' H_2	ν WB	Berkeley, Fermilab, Hawaii, Michigan	[6]
15' Ne-H_2	$\bar{\nu}$ (ν) WB	Fermilab, IHEP, ITEP, Michigan	[7-19]
15' Ne-H_2	ν WB	Berkeley, Fermilab, Hawaii, Seattle, Wisconsin	[20]
15' D_2	ν WB	Illinois-Tech, Maryland, Sendai, Stony Brook, Tufts	[21-26]
BEBC Ne-H_2	ν,$\bar{\nu}$ NB	Aachen, Bonn, CERN, Demokritos, IC London, Oxford, Saclay	[27,28]
BEBC H_2	ν,$\bar{\nu}$ WB	Aachen, Bonn, CERN, Munich, Oxford	[29-38]
BEBC D_2	$\bar{\nu}$ (ν) WB	Amsterdam, Bologna, Padova, Pisa, Saclay, Torino	[39,40]
BEBC Ne-H_2	$\bar{\nu}$ WB	Bari, Birmingham, Brussels, CERN, Demokritos, Ecole Polytechnique, IC London, Munich, Oxford, RHEL, Saclay, UC London	[41]
GGM Propan, Freon	ν WB	CERN, Milano, Orsay	[42]
SKAT Freon	ν,$\bar{\nu}$ WB	IHEP, Berlin-Zeuthen	[43,44]

Most features of hadron production by neutrinos and antineutrinos can be successfully described in the frame work of the quark-parton model (QPM) which is shown in Fig.1. For some purposes (e.g. scaling-violation, non-factorisation, transverse momentum and jet properties) the simple version of the model has to be extended by gluon effects as described by quantum-chromodynamics (QCD). Neglecting the sea quarks and the Cabibbo angle one encounters in νN and $\bar{\nu}N$ scattering, in contrast to charged-lepton nucleon scattering ($eN, \mu N$), a very clean and simple flavor situation:

In neutrino scattering a d-quark of the incident nucleon absorbs the positive current (W^+) and becomes a forward-going (i.e. in current direction) u-quark which then hadronizes into the current fragments. The unaffected diquark (uu for a proton target, ud for a neutron target) travels backward as a spectator and fragments into the target fragments+). Thus in νp (νn) scattering the fragmentation functions $D_u^h(z,p_T)$ and $D_{uu}^h(z,p_T)$ ($D_{ud}^h(z,p_T)$) of the u-quark and the uu-diquark (ud-diquark), respectively, into hadrons of a particular type h can be studied. Here z is the energy or momentum fraction carried by the hadron (see below) and p_T the transverse momentum of the hadron, measured with respect to the current direction.

In antineutrino scattering on the other hand, the negative current (W^-) is absorbed by a u-quark of the incident nucleon and the partonic final state consists of a forward-going d-quark and a backward-going ud-diquark or dd-diquark for $\bar{\nu}p$ or $\bar{\nu}n$ scattering, respectively. Here the fragmentation functions $D_d^h(z,p_T)$ and $D_{ud}^h(z,p_T)$ for $\bar{\nu}p$ ($D_{dd}^h(z,p_T)$ for $\bar{\nu}n$) can be investigated.

The event and particle variables used to describe the leptoproduction of hadrons are well known:

<u>Event variables</u>:

W = effective mass of all secondary hadrons

(2a) $$W^2 = M^2 + 2M\nu - Q^2 = M^2 + 2ME_\nu y - Q^2 = M^2 + Q^2\left(\frac{1}{x} - 1\right).$$

Q^2 = four-momentum transfer squared.

+) In the context of the QPM it would be more appropriate to speak of "quark fragments" and "diquark fragments" instead of using the common notation "current fragments" and "target fragments", respectively.

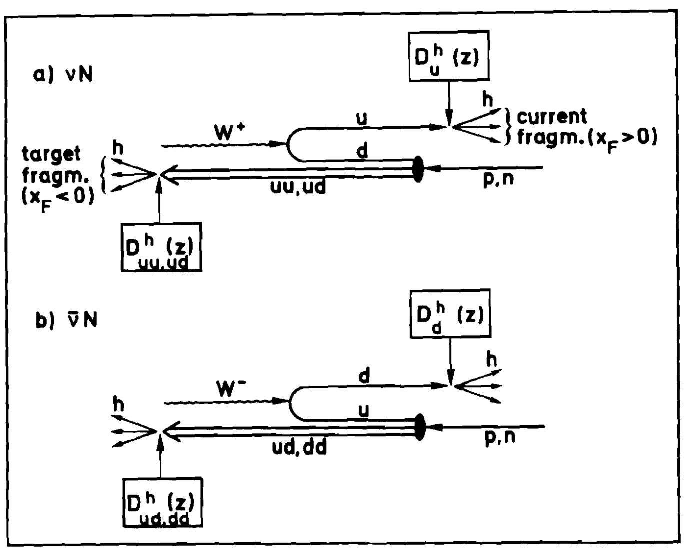

Fig. 1

The quark-parton model (QPM) for neutrino and antineutrino scattering on protons and neutrons.

(2b) $\nu = E_\nu - E_\mu = E_H - M$ = lab energy of the exchanged vector boson $W^\pm$, where E_ν, E_μ, E_H are the lab energy of neutrino, muon and all secondary hadrons, respectively, and M = nucleon mass.

(2c) $x = \frac{Q^2}{2M\nu} = \frac{Q^2}{2ME_\nu y}$ = Bjorken-x.

(2d) $y = \frac{\nu}{E_\nu}$ = relative energy transfer.

Particle variables:

(3a) $x_F = \frac{p_L^*}{p_{Lmax}^*}$ = Feynman-x $\approx \frac{p_L^*}{W/2}$, where p_L^* is the longitudinal momentum of the particle in the cm system of all secondary hadrons, and p_{Lmax}^* its maximum kinematical value.

(3b) z = energy fraction = $\frac{E}{\nu}$ or $\frac{E}{E_H}$ or $\frac{E^*}{W/2}$, where E (E^*) is the lab (cms) energy of the particle.

p_T = transverse momentum with respect to the current direction.

At high energies the various definitions of z are equivalent for current fragments.

A separation of the current and target fragments is possible, at least approximately, at higher values of W ($W \gtrsim 4$ GeV), whereas at low W current and target fragments overlap in momentum space [2]. It turns out [46] that the cm system of all secondary hadrons is most appropriate to carry out this separation at high W by selecting as current (target) fragments those hadrons, which go forward (i.e. $x_F > 0$)(backward, i.e. $x_F < 0$) in the hadronic cms.

According to the new results as obtained by the various experiments, this review will cover the following topics:

- Multiplicities
- Forward net charge and charge distributions
- Fragmentation functions
- Transverse momentum and jet properties.

We will not discuss the production of strange particles [3-5,10,11,13,25,26,34]; it is partially related to the production of charmed particles which is treated in the talk of E. Fisk.

B.) Multiplicities

In this chapter we discuss preferentially the "clean" cases of $\nu p, \bar{\nu}p, \nu n$ and $\bar{\nu}n$ scattering at high energies leaving out some new data [13,43,44] obtained on isoscalar targets (νN and $\bar{\nu}N$). The following main results on multiplicity have been obtained by the various experiments:

1.) Within the available W ranges, the average charged multiplicity $\langle n \rangle$ rises linearly with $\ln W^2$ for $W \gtrsim 2$ GeV.

Linear fits of the form

(4) $\langle n \rangle = a + b \cdot \ln W^2$

have been carried out by the various experiments; the fitted values for a and b are summarized in Table 2. The fitted straight lines representing the data in the respective W^2 intervals are shown by the straight lines in Fig. 2. The two νp lines are in good agreement with each other, although their intercept values a are quite different (Table 2). As for $\bar{\nu}p$ there seems to be some disagreement between the two experiments [4,40] which lies mainly in the data points at low W^2 ($\lesssim 10$ GeV^2). It should be noted that for $\bar{\nu}p$ scattering (with hadronic charge $Q_H = 0$) the total event number is hard to determine since

Table 2: Compilation of values for a and b obtained from fitting $\langle n \rangle = a + b \cdot \ln W^2$ (W in GeV) to the average charged multiplicity $\langle n \rangle$ vs. W^2.

Reaction	Hadronic charge Q_H	W^2 range (GeV^2)	a	b	Reference
νp	2	4 - 200	0.37 ± 0.02	1.33 ± 0.02	[32]
		4 - 100	0.80 ± 0.10	1.25 ± 0.04	[21]
$\bar{\nu} p$	0	4 - 100	-0.44 ± 0.13	1.48 ± 0.06	[4]
		6 - 140	0.18 ± 0.20	1.23 ± 0.07	[40]
νn	1	4 - 100	0.21 ± 0.10	1.21 ± 0.04	[21]
$\bar{\nu} n$	-1	4 - 140	0.79 ± 0.09	0.93 ± 0.04	[40]

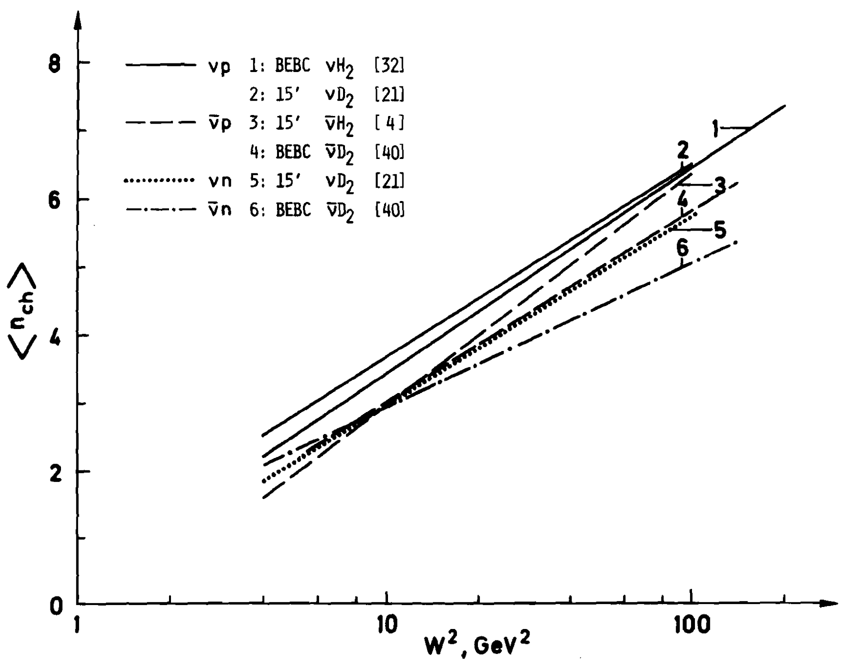

Fig. 2

Average charged multiplicity $\langle n \rangle$ vs. W^2. The straight lines show linear fits of the form $\langle n \rangle = a + b \cdot \ln W^2$ to the data points from various experiments. The fitted values for a and b are compiled in Table 2.

here the one-prong channel $\bar{\nu} p \to \mu^+ +$ neutrals contributes, mainly at low W. This channel is difficult to detect and identify in the bubble chamber. Therefore the discrepancy between the two experiments is probably due to different detection efficiencies for the one-prong channel and to different procedures applied to correct for these scanning losses.

From Fig. 2 the following regularity seems to appear at higher W:

(5) $$\langle n \rangle_{\nu p} > \langle n \rangle_{\bar{\nu} p} \approx \langle n \rangle_{\nu n} > \langle n \rangle_{\bar{\nu} n}$$

where the approximate equality $\langle n \rangle_{\bar{\nu} p} \approx \langle n \rangle_{\nu n}$ is expected from the QPM (Fig.1): For both reactions the diquark (containing mostly the final-state baryon amongst its fragments) is the same (namely ud) and $d \to h^{\pm}$ (for $\bar{\nu} p$) is the same as $u \to h^{\mp}$ (for νn) for pion fragments due to isospin symmetry.

From Fig. 2 it is not yet clear whether all four multiplicities $\langle n \rangle$ rise with the same slope b (~ 1.3); more precise measurements, in particular on neutron targets, are needed.

It is found [1,26,37] that also the average multiplicity of ρ^0 mesons rises with W. The BEBC νH_2 collaboration [37] for example obtains the following linear fit to their data points between $10 \lesssim W^2 \lesssim 200$ GeV^2:

(6) $$\langle n_{\rho^0} \rangle = (-0.08 \pm 0.12) + (0.085 \pm 0.045) \cdot \ln W^2 .$$

2.) At fixed W, $\langle n \rangle$ is almost independent of Q^2 (not shown) [4,13,32,40].

3.) The dispersion $D = \sqrt{\langle n^2 \rangle - \langle n \rangle^2}$ of the charged-multiplicity distribution rises linearly with $\langle n \rangle$ (Wroblewski relation [47]).

Linear fits of the form

(7) $$D = a + b \langle n \rangle \quad \text{or} \quad D_- = a_- + b_- \langle n_- \rangle \qquad (\text{with } b = b_-)$$

(where n_- is the negative multiplicity and D_- the dispersion of its distribution) have been carried out by the various collaborations; the fitted values obtained for a_- and b_- are compiled in Table 3. The fitted straight lines D_- vs. $\langle n_- \rangle$ are shown in Fig. 3. Again a discrepancy between the two $\bar{\nu}p$ experiments [4,40] is observed.

As Fig. 4 shows the question as to whether the dispersion rises with the same slope b (~ 0.35) for all four reactions is not yet settled. In $\bar{p}p$ annihilation a slope of b = 0.37 has been observed [48]. Furthermore Wroblewski has found [49] that also in hadron-hadron collisions (e.g. pp), after subtracting the contribution of diffractive scattering, the multiplicity dispersion rises with a slope of $b \approx 0.36$.

4.) The charged-multiplicity distribution obeys Koba-Nielsen-Olesen (KNO) [50] scaling.

In Fig. 4 the scaled multiplicity distribution $\langle n \rangle \cdot P(n,W)$ is plotted vs. $n/\langle n \rangle$ for four W intervals for $\bar{\nu}p$ and $\bar{\nu}n$ scattering from the BEBC $\bar{\nu}D_2$ experiment [40]. Here P(n,W) is the normalized charged-multiplicity distribution with $\Sigma P(n,W) = 1$. Independence of W, i.e. KNO scaling is observed both for $\bar{\nu}p$ (full^n symbols) and $\bar{\nu}n$ (open symbols) scattering. Furthermore the KNO distributions for $\bar{\nu}p$ and $\bar{\nu}n$ seem to coincide.

KNO scaling has been observed previously in νp [21,32] and νn [21] scattering, with good agreement between the 15' νD_2 [21] and BEBC νH_2 [32] experiments on the KNO distribution for νp scattering. Furthermore the 15' νD_2

Table 3: Compilation of values for a_- and b_- obtained from fitting $D_- = a_- + b_- \langle n_- \rangle$ to the negative dispersion D_- vs. the average negative multiplicity $\langle n_- \rangle$.

Reaction	Hadronic charge	$\langle n_- \rangle$ range	a_-	b_-	Reference
νp	2	0.5 - 2.7	0.36 ± 0.03	0.36 ± 0.03	[32]
		0.4 - 2	0.42	0.34 ± 0.01	[21]
$\bar{\nu}p$	0	0.5 - 3.0	0.34	0.31 ± 0.12	[4]
		1 - 2.7	0.16 ± 0.11	0.42 ± 0.06	[40]
νn	1	0.5 - 2.1	0.41	0.34 ± 0.01	[21]
$\bar{\nu}n$	-1	1.3 - 2.7	-0.22 ± 0.10	0.49 ± 0.05	[40]

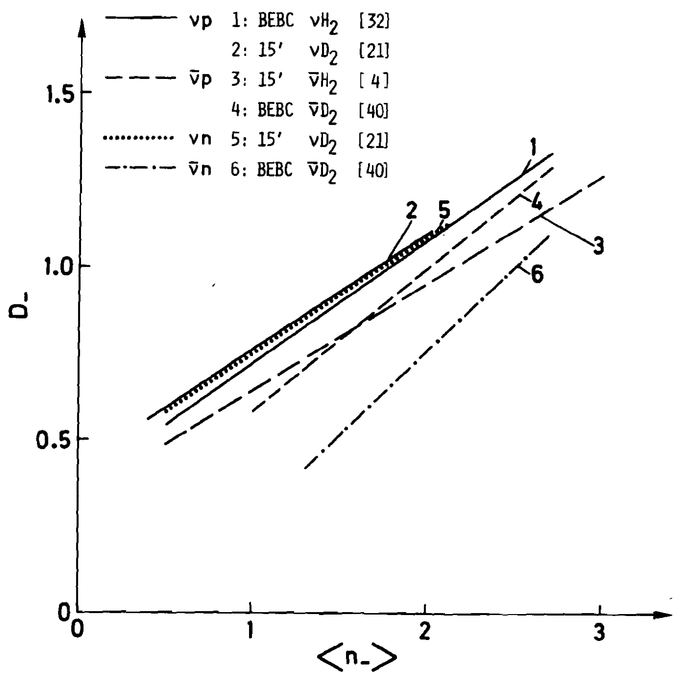

Fig. 3

Dispersion D_- as a function of $\langle n_- \rangle$. The straight lines show linear fits of the form $D_- = a_- + b_- \cdot \langle n_- \rangle$ (equ. (7)) to the data points from various experiments. The fitted values for a_- and b_- are compiled in Table 3.

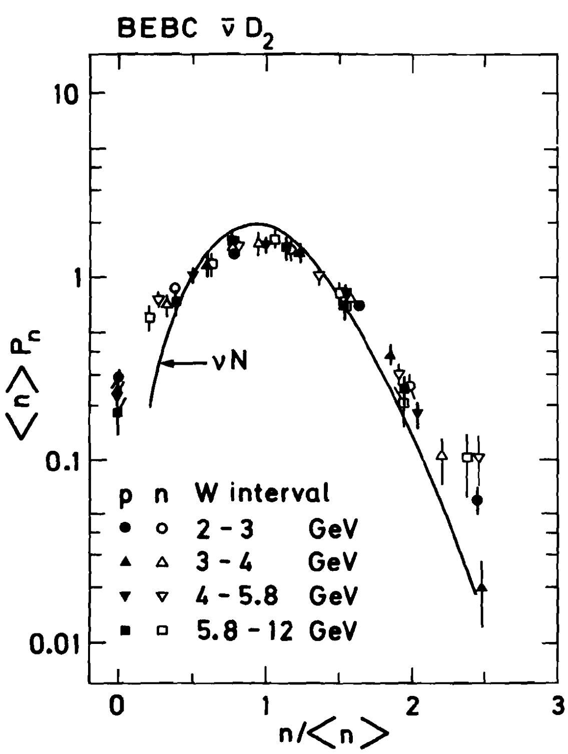

Fig. 4

KNO-distribution $\langle n \rangle P(n,W)$ vs. $n/\langle n \rangle$ for four W intervals for $\bar{\nu}p$ (full symbols) and $\bar{\nu}n$ (open symbols) scattering, from BEBC $\bar{\nu}D_2$ [40]. The curve shows an eyeball fit to the νp and νn KNO distributions from 15' νD_2 [21] and BEBC νH_2 [32].

experiment has shown, that the KNO distributions for νp and νn are the same. An eyeball fit through the νN KNO distributions from both experiments is given by the curve in Fig. 4. It is seen that the KNO distribution is wider for $\bar{\nu}N$ (data points) than for νN (curve). At present we have no simple explanation for this difference.

The 15' $\bar{\nu}Ne$-H_2 collaboration [13] has shown that KNO scaling holds separately for the multiplicity of charged hadrons going forward in the hadronic cms (see Fig. 5).

5.) In the average, more charged hadrons are produced in the forward than in the backward cms hemisphere.

This has been observed by the BEBC νH_2 [32], 15' νD_2 [23], 15' $\bar{\nu}H_2$ [3] and BEBC $\bar{\nu}D_2$ [40] collaborations. As an example, Fig. 6 shows the average forward and backward multiplicities vs. W^2 for $\bar{\nu}p$ [3,40] and $\bar{\nu}n$ [40]. A possible explanation for the abundance of forward-going hadrons is the fact that the baryon (mainly proton or neutron) in the reaction is emitted predominantly in the backward direction as the leading particle carrying a sizeable fraction of the available backward energy and thus leaving less energy for the production of additional backward-going hadrons. In the QPM the difference in forward and backward multiplicity implies a difference in quark and diquark fragmentation.

6.) At W around 8 GeV, no strong correlations exist between the charged multiplicities in the forward and backward cms hemispheres.

Fig. 7 shows $\langle n_F \rangle$ vs. n_B and vice versa for three W intervals from the BEBC νH_2 experiment. $\langle n_F \rangle$ is seen to be rather independent of n_B at $W \approx 8$ GeV (and vice versa). This independence is expected from the QPM which predicts the current quark and the diquark to fragment independently from each other.

Wroblewski [51] has observed a linear relation

$$\langle n_F \rangle = a + b \cdot n_B \tag{8}$$

in pp scattering at the high ISR energies where the slope b is positive and increases with energy ($\propto \ell ns$). A value of $b \approx 0$ as observed in Fig. 7 at $W \approx 8$ GeV fits nicely into his plot of b vs. ℓns. From this possible pp and νN similarity one would expect $\langle n_F \rangle$ to rise with n_B (and vice versa) also in νN scattering at higher W values where at present no sufficiently accurate data are available. Such a trend with W (i.e. $b < 0$ at low W, $b \approx 0$ at $W \approx 8$ GeV and $b > 0$ at high W) is indeed suggested by the data points in Fig. 7.

7.) The average π^0 multiplicity rises with increasing charged multiplicity.

Fig. 8 shows $\langle n_{\pi^0} \rangle$ vs. n_- for $\bar{\nu}N$ and νN scattering from the 15' $\bar{\nu}$, νH_2 [4]

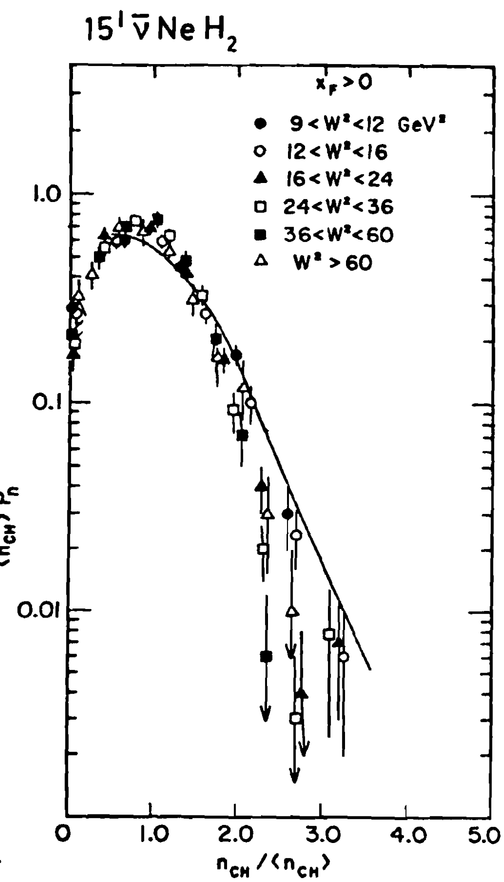

Fig. 5

KNO-distribution for charged hadrons going forward in the hadronic cms for six W intervals in $\bar{\nu}N$ scattering, from 15' $\bar{\nu}Ne$-H_2 [13]. The curve represents a fit to π^+p and $\bar{p}p$ data.

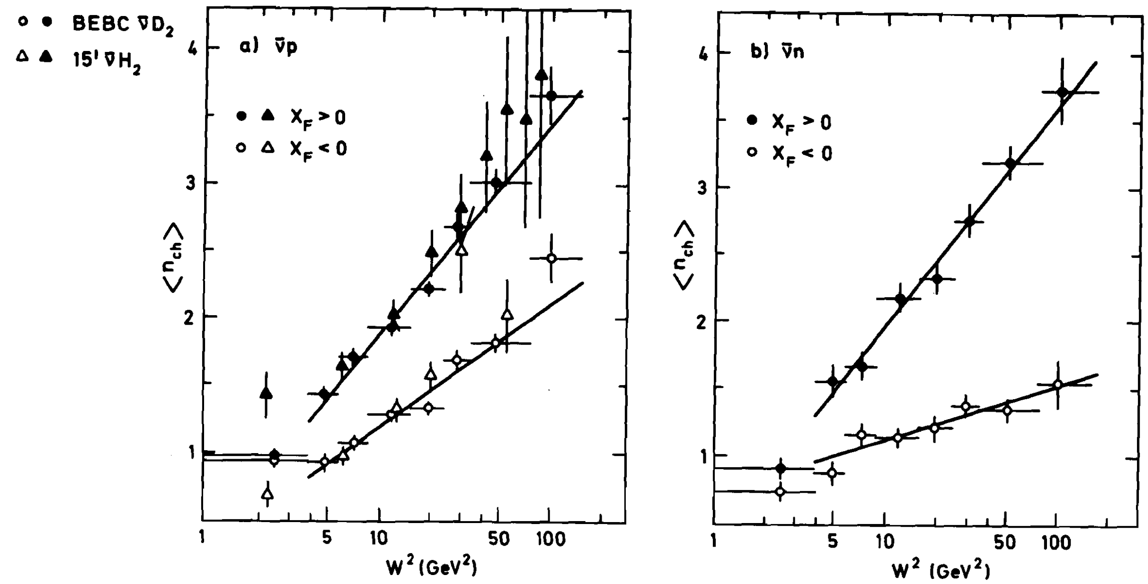

Fig. 6
Average charged multiplicity in the forward (x_F > 0) and backward (x_F < 0) hemisphere in the hadronic cms vs. W^2, (a) for $\bar{\nu}p$ and (b) $\bar{\nu}n$ scattering, from BEBC $\bar{\nu}D_2$ [40] (circles) and 15' $\bar{\nu}H_2$ [3] (triangles). The straight lines show linear fits to the data points of ref. [40].

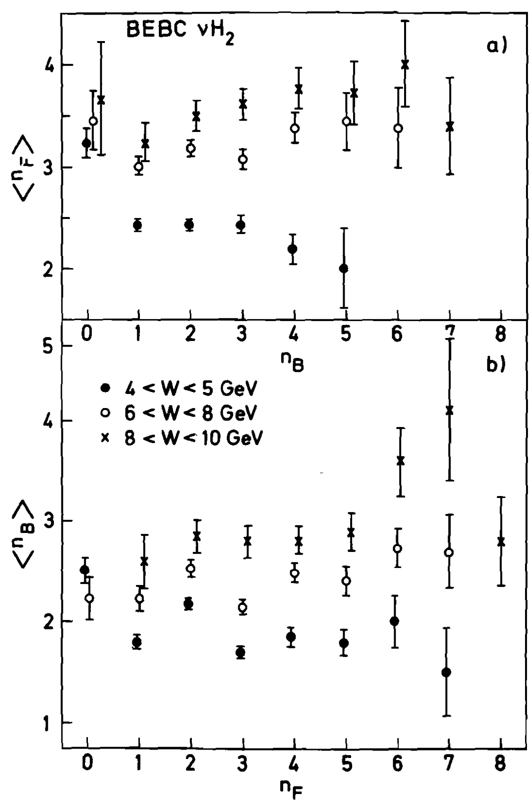

Fig. 7
(a) Average forward multiplicity $\langle n_F \rangle$ vs. backward multiplicity n_B and (b) average backward multiplicity $\langle n_B \rangle$ vs. forward multiplicity n_F for charged hadrons in νp scattering for three W intervals, from BEBC νH_2.

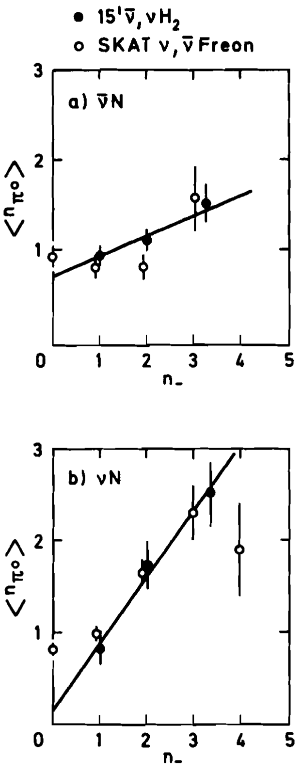

Fig. 8
Average π^o multiplicity $<n_{\pi^o}>$ vs. negative multiplicity n_- for (a) $\bar{\nu}$N and (b) νN scattering, from 15' $\bar{\nu}$,νH_2 [4] (full points) and SKAT ν,$\bar{\nu}$ Freon [43] (open circles). The straight lines are linear fits to the full points, see equ. (9).

and SKAT ν,$\bar{\nu}$ Freon [43] experiments. The straight lines are linear fits to the data points of ref. [4] yielding

(9)
$$<n_{\pi^o}> = (0.72 \pm 0.18) + (0.22 \pm 0.10)n_- \quad \text{for } \bar{\nu}p$$
$$<n_{\pi^o}> = (0.14 \pm 0.30) + (0.73 \pm 0.16)n_- \quad \text{for } \nu p$$

A possible explanation for the observed π^o-$\pi^\pm$ correlation could be the production of meson resonances (e.g. $\rho^\pm \to \pi^\pm\pi^o$, $\omega \to \pi^+\pi^-\pi^o$).

C.) Forward net charge and charge distributions

As Field and Feynman [52] have shown, the average charge $<Q_q>$ of mesons (neglecting baryon fragments) from the fragmentation of a quark q is related to the charge e_q of this fragmenting quark by

(10) $$<Q_q> = e_q - \sum_a \gamma_a e_a \quad .$$

Here γ_a is the probability to create a quark-antiquark pair $a\bar{a}$ from the "sea" in the fragmentation process and the sum extends over all quark flavors. The second term, called the "leakage term", arises for the following reason: In the fragmentation process neutral quark-antiquark pairs are created from the "sea" which together with the original quark form the observed meson fragments. Therefore the quark a of the last pair $a\bar{a}$ in the fragmentation chain, created with probability γ_a, has to be excluded and its charge must be subtracted.

Neglecting heavy quark pairs ($\gamma_c = \gamma_b = 0$), assuming $e_u-e_d = 1$ (π^+) and $e_u-e_s = 1$ (K^+), and using $\gamma_u + \gamma_d + \gamma_s = 1$ one obtains from equ. (10):

(11) $$<Q_u> = 1-\gamma_u \quad \text{and} \quad <Q_d> = <Q_s> = -\gamma_u \quad .$$

It is thus the probability γ_u and not the quark charges which one obtains from measuring $<Q_u>$ and $<Q_d>$.

The quantities $<Q_u>$ and $<Q_d>$ can be determined in νN and $\bar{\nu}$N scattering, respectively, by measuring the average net charge

(12) $$<Q_F> = (N_F^+ - N_F^-)/N_{ev}$$

of forward-going hadrons, i.e. of the current fragments (Fig.1). $N_F^\pm$ is the number of positive and negative hadrons going forward ($x_F > 0$) in the hadronic cms. However, at finite W there is a kinematical overlap with the target fragments. Therefore, the forward net charge $<Q_F>$ is usually plotted vs. 1/W and a linear extrapolation, justified by a correlation-length argument [7], is carried out towards $1/W = 0$ where the overlap of current and target fragments has disappeared. The values $<Q_F>^{\nu N}$ and $<Q_F>^{\bar{\nu}N}$ at $W = \infty$ are then identified with $<Q_u>$ and $<Q_d>$, respectively, such that

(13) $$\gamma_u = 1 - <Q_F>^{\nu N} = - <Q_F>^{\bar{\nu}N}$$

from equ. (11). In addition, a cut in Bjorken-x is usually applied in order to remove a contamination from sea quarks in the nucleon.

The values for $<Q_F>^{\nu N}$ and $<Q_F>^{\bar{\nu}N}$ as obtained by various experiments [3,7,12, 32,40] from extrapolating to $W = \infty$ are compiled in Table 4 together with the resulting values of γ_u. The γ_u values are also plotted in Fig.9. It is seen that some values, although with larger errors, fall above the theoretical boundary $\gamma_u \leqslant 0.5$ which follows from $\gamma_u + \gamma_d + \gamma_s = 1$ and assuming

Table 4: Compilation of average forward net charges, extrapolated to $W = \infty$, in νN and $\bar{\nu} N$ scattering and corresponding values of $\gamma_u = 1 - \langle Q_F \rangle^{\nu N} \doteq - \langle Q_F \rangle^{\bar{\nu} N}$, equ.(13).

Selection on Bjorken-x	$\langle Q_F \rangle^{\nu N}$	$\langle Q_F \rangle^{\bar{\nu} N}$	γ_u	reference
x > 0.10		-0.44 ± 0.09 ($\bar{\nu}N$)	0.44 ± 0.09	[7,12]
	0.54 ± 0.12 (νN)		0.46 ± 0.12	
all x		-0.69 ± 0.16 ($\bar{\nu}p$)	0.69 ± 0.16	[3]
	0.40 ± 0.17 (νp)		0.60 ± 0.17	
all x	0.67 ± 0.10 (νp)		0.33 ± 0.10	[32]
all x		-0.38 ± 0.07 ($\bar{\nu}p$)	0.38 ± 0.07	[40]
		-0.60 ± 0.11 ($\bar{\nu}n$)	0.60 ± 0.11	
		-0.47 ± 0.06 ($\bar{\nu}D$)	0.47 ± 0.06	
x > 0.15		-0.38 ± 0.09 ($\bar{\nu}D$)	0.38 ± 0.09	

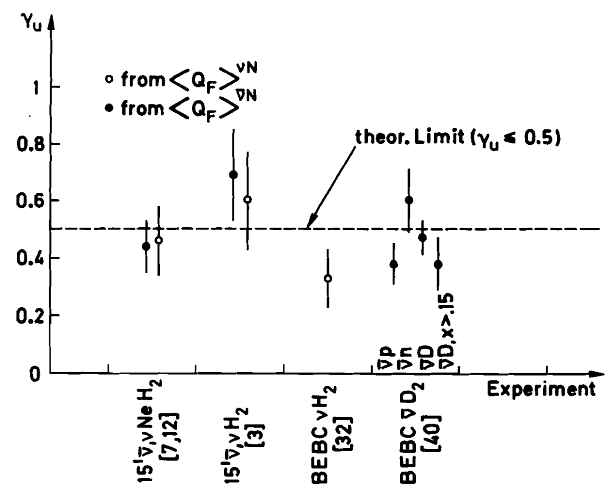

Fig. 9

Values obtained for γ_u, the probability to create a $u\bar{u}$ pair from the sea, by various experiments (Table 4). The values were obtained by extrapolating the average forward net charge $\langle Q_F \rangle$ in νN and $\bar{\nu} N$ scattering to $W = \infty$ and using $\gamma_u = 1 - \langle Q_F \rangle^{\nu N} = -\langle Q_F \rangle^{\bar{\nu} N}$, equ.(13).

$$\gamma_u = \gamma_d \equiv \gamma \tag{14}$$

because of isospin symmetry. The average over all experiments is $\gamma_u = 0.45 \pm 0.04$ where for the BEBC $\bar{\nu} D_2$ experiment [40] an average of the two $\bar{\nu} D$ values has been used.
This yields $\gamma_s/\gamma = 0.22 \pm^{0.22}_{0.18}$ with a rather large error and in agreement with the much more precise value of $\gamma_s/\gamma = 0.27 \pm 0.04$ as determined in ref.[8] directly by comparing the d-quark fragmentation into K^0 ($= d\bar{s}$) and into π^- ($= d\bar{u}$) at large z. For an SU(3)-symmetric sea one would of course expect $\gamma_u = \gamma_d = \gamma_s$, i.e. $\gamma_s/\gamma = 1$.

In order to avoid a contamination of current fragments by target fragments Field and Feynman [52] have proposed an alternative method. It consists in measuring for each event a weighted charge

$$Q_W = \sum_i z_i^r Q_i \tag{15}$$

where z_i is the energy fraction (equ. (3b)) carried by the ith hadron, Q_i its charge and r a small positive number. By this weighting procedure a hadron which is close to the fragmenting quark (i.e. with a large z) gets a stronger weight than a hadron which is further down in the fragmentation chain or is even a target fragment.

Distributions of Q_W, normalized to unity, have been measured by the 15' $\bar{\nu}$, νNe-H_2 [12,16] and BEBC $\bar{\nu} D_2$ [40] collaborations for events with high W; they are shown for $r = 0.5$ in Figs.10 and 11, respectively, and are compared with the predicted distributions of Field and Feynman [52] for a quark jet of 10 GeV. It is seen that, as expected, in case of $\nu N(\bar{\nu}N)$ scattering the measured Q_W distribution is in nice agreement with the prediction for a u-quark (d-quark) jet and not with that for a d-quark (u-quark) jet.

D.) Fragmentation functions

Fragmentation functions of quarks and diquarks, i.e. distributions of the energy fraction z or of the longitudinal-momentum fraction x_F,

$$(16)\qquad D^h(z) = \frac{1}{N_{ev}}\frac{dN^h}{dz} \quad \text{or} \quad D^h(x_F) = \frac{1}{N_{ev}}\frac{dN^h}{dx_F},$$

for hadrons of a particular type h have been measured in practically all experiments listed in Table 1 [1-3,5,6,10,11,13,17,24-26,28,34,36,37,39,41-44]; they cannot all be shown here. It is worth mentioning that apart from the z or x_F distributions of positive and negative hadrons $h^\pm$ (mainly $\pi^\pm$) also those of π^0 [43], strange particles [3,5,10,11,13,25,26,34] and ρ^0 mesons [1,6,26,37] have been determined.

We now discuss the most important properties of fragmentation functions, as they have been studied recently.

1.) Universality

According to the simple QPM the fragmentation of a final-state quark should be independent of the type of interaction, from which this fragmenting quark originates (universality, environmental independence [53,54]). Thus the fragmentation functions as measured in $\nu N, \bar{\nu}N, eN, \mu N$ scattering and in e^+e^- annihilation are predicted to be the same. It is known since some time [55,46] that this prediction is (nearly) fulfilled. Fig. 12 of the 15'$\bar{\nu}$Ne-H_2 collaboration [13] shows a more recent compilation of z distributions as measured in various processes: forward-going charged hadrons (pions) from $\bar{\nu}N$ and ep scattering, π^0 from ep scattering (multiplied by 2 assuming $2N^{\pi^0} = N^{\pi^+} + N^{\pi^-}$), and charged hadrons from pp scattering

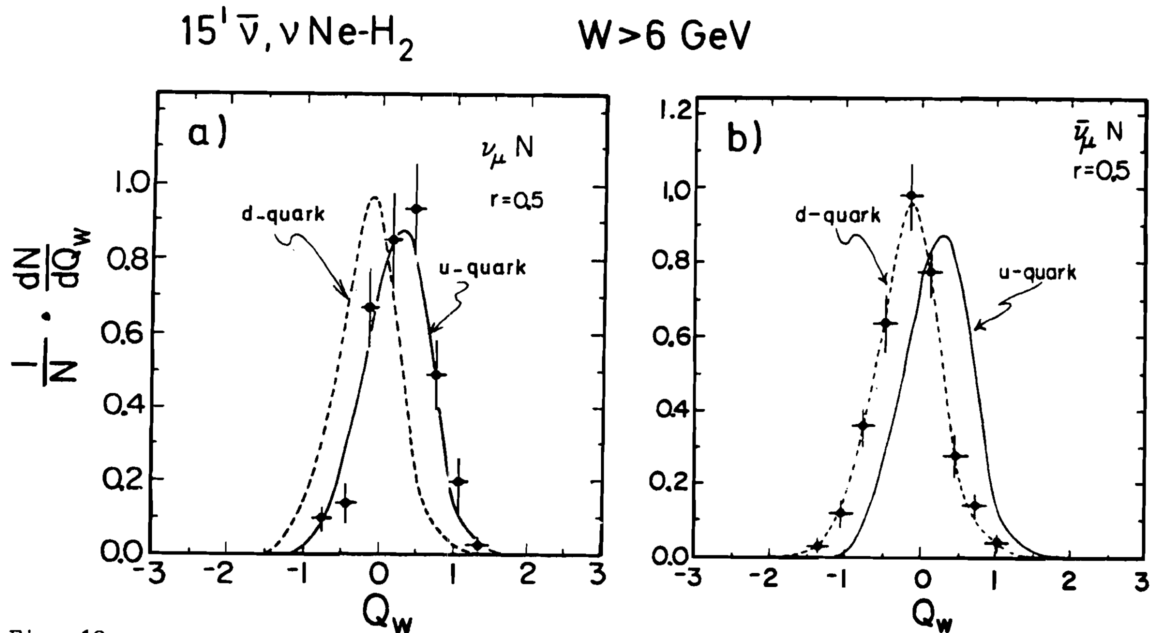

Fig. 10

Distributions of weighted charge Q_W (equ.(15) with $r = 0.5$), normalized to unity, for (a) νN and (b) $\bar{\nu}N$ scattering with $W > 6$ GeV, from 15' $\bar{\nu}$,νNe-H_2 [12,16]. The curves show the predictions of Field and Feynman [52] for a u-quark and d-quark jet of 10 GeV.

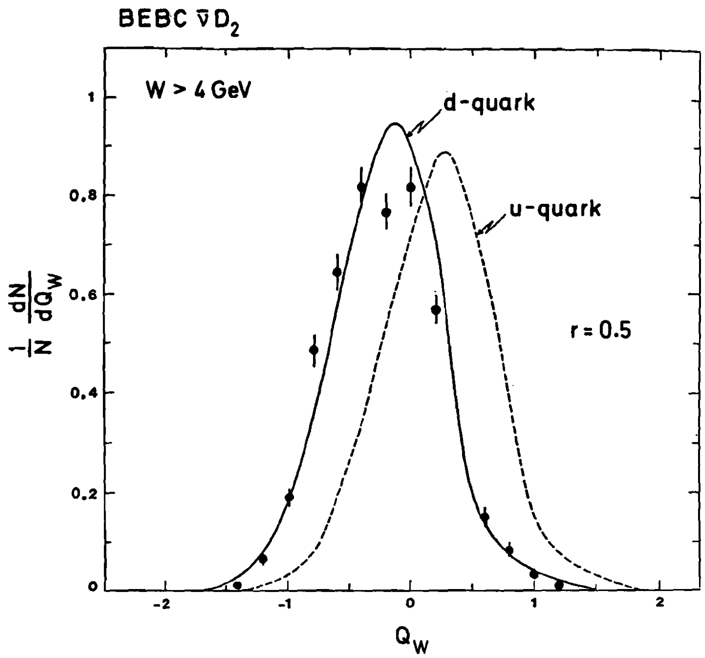

Fig. 11

Distribution of weighted charge Q_W (equ. (15) with $r = 0.5$), normalized to unity, for $\bar{\nu}N$ scattering with $W > 4$ GeV, from BEBC $\bar{\nu}D_2$ [40]. The curves show the predictions of Field and Feynman [52] for a u-quark and d-quark jet of 10 GeV.

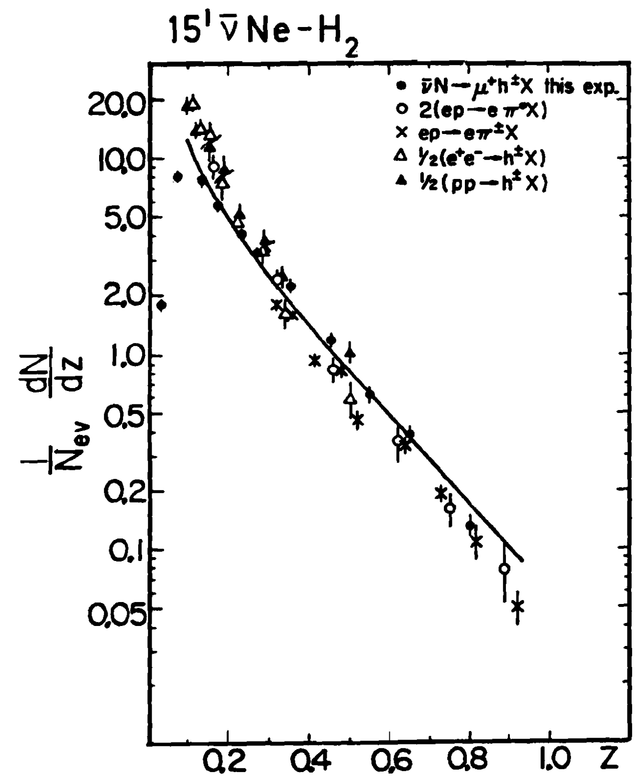

Fig. 12

Distributions of the energy fraction z for forward-going charged hadrons (pions) in $\bar{\nu}N$, ep and pp (ISR) scattering and in e^+e^- annihilation, and of π^0 in ep scattering, from 15'$\bar{\nu}$Ne-H_2 [13].

and e^+e^- annihilation (both multiplied by 1/2 in order to take only one hemisphere). It is seen that all z-distributions roughly coincide as expected [53].

2.) Isospin relations

Isospin symmetry predicts certain relations amongst fragmentation functions [53]. As an example, Fig. 13 shows a test of the relation

$$D_u^{\pi^\pm}(x_F) = D_d^{\pi^\mp}(x_F) \tag{17}$$

by the BEBC $\nu,\bar{\nu}H_2$ collaboration [36], where the u-quark and d-quark fragmentation functions are measured in νp and $\bar{\nu}p$ scattering, respectively. It is seen that in the current-fragmentation region ($x_F > 0$) the invariant x_F distributions for π^+ (after correcting for unidentified protons) from νp (full points) and for π^- from $\bar{\nu}p$ (open circles) agree nicely with each other, as predicted.

A further example of an isospin relation for diquark fragmentation will be given in the following section.

3.) Diquark fragmentation

As explained in the Introduction (Fig. 1), diquark fragmentation functions can be determined by measuring the x_F distributions in the backward hemisphere ($x_F<0$). As an example, Fig. 14a from the BEBC νH_2 experiment [36] shows the backward x_F distribution of π^+ (after correcting for unidentified protons) and π^- in νp scattering, and Fig. 14b from the 15' $\bar{\nu}H_2$ experiment [3] the backward x_F distribution of h^+ (after removing identified protons) and h^- in $\bar{\nu}p$ scattering. From Fig. 14a it is seen that $D_{uu}^{\pi^+} > D_{uu}^{\pi^-}$. This is expected, since the π^+ can be the leading particle containing a u-quark from the fragmenting uu-diquark and thus carrying a larger momentum fraction, whereas the π^- contains only quarks created later on in the fragmentation process from the sea. In $\bar{\nu}p$ scattering on the other hand (Fig. 14b) the π^+ and π^- distributions are rather equal. This is again expected in the QPM (Fig. 1), since isospin symmetry predicts $D_{ud}^{\pi^+} = D_{ud}^{\pi^-}$.

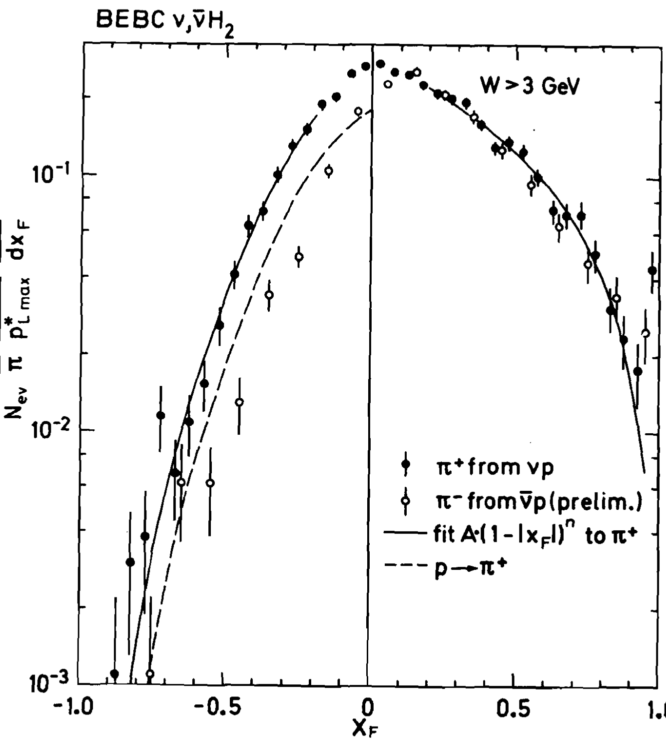

Fig. 13

Normalized invariant x_F distributions of π^+ (after correcting for unidentified protons) in νp (full points) and of π^- in $\bar{\nu}p$ (open circles) scattering with W > 3 GeV. The full curves show fits of the form $A\cdot(1-|x_F|)^n$ to the π^+ points for $|x_F| > 0.2$ in each hemisphere, with $n = 1.23 \pm 0.05$ for $x_F > 0.2$ and $n = 3.45 \pm 0.15$ for $x_F < -0.2$. The dashed curve represents the invariant x_F distribution for π^+ from a pp experiment [56]. From BEBC νH_2 [36].

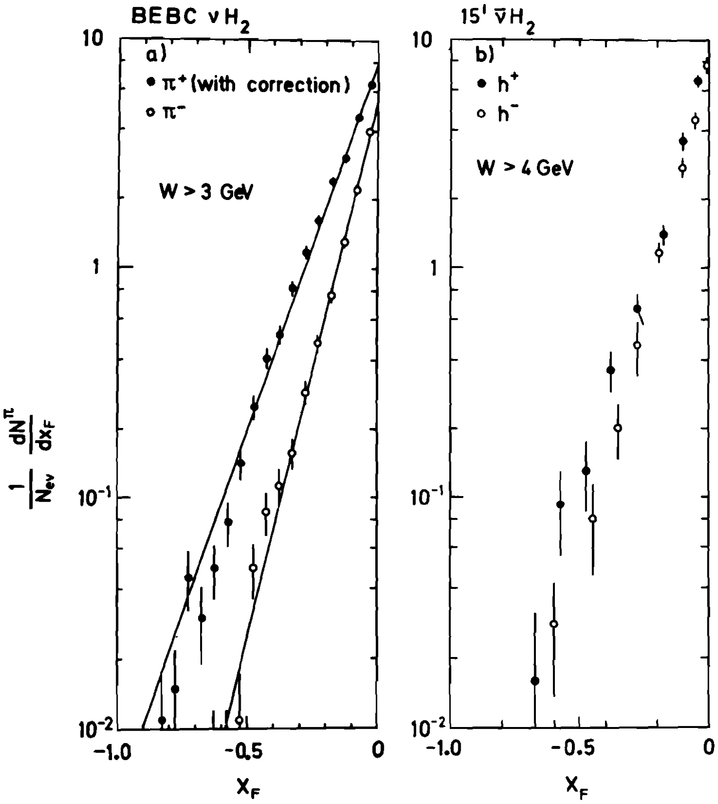

Fig. 14
(a) normalized x_F distribution of backward-going π^+ (after correcting for unidentified protons) and π^- in νp events with W > 3 GeV, from BEBC νH_2 [36]; (b) normalized x_F distribution of backward-going positives (after removing identified protons) and negatives in $\bar{\nu}p$ events with W > 4 GeV, from 15' $\bar{\nu}H_2$ [3].

4.) Scaling violation

The question of scaling violation of fragmentation functions has been investigated in various experiments [57,2,28,29,39]. A scaling violating Q^2 dependence of the z-distributions is observed, when all values of W are included, whereas the z-distributions turn out to be independent of Q^2, if only events with larger W ($\gtrsim$ 4 GeV) are taken. Fig. 15 from the BEBC $\bar{\nu}D_2$ experiment [39] shows a recent measurement of the z-distributions of π^+ and π^- for two Q^2 regions. If all W are taken (Fig. 15a,b), the distributions are steeper at high Q^2 than at low Q^2, whereas they do not depend on Q^2 for events with W > 4 GeV (and forward-going particles, x_F > 0) (Fig. 15c,d).

A quantitative comparison of the observed Q^2 dependence with the predictions of perturbative QCD has been carried out in terms of moments of fragmentation functions. It is found [57,28,29] that in case of neutrino scattering the agreement with QCD is surprisingly good. For antineutrino scattering on the other hand the Q^2 dependence of the non-singlet (NS) moments cannot be described by QCD [2,28]. An explanation for this difficulty may be the fact that the NS-moments in $\bar{\nu}N$ are much smaller than in νN scattering, so that effects other than QCD play a relatively more important role for the $\bar{\nu}N$ than for the νN NS-moments. However, it is probably fair to say, that the observed Q^2 dependence and its disappearance for higher W is not yet really well understood.

5.) Non-factorisation in x and z

The semi-inclusive cross section for the production of a hadron h in the reactions (1) can in general be written as a product of the event cross section times a generalized fragmentation function $D^h(x,z,Q^2)$:

$$\frac{d\sigma^h}{dx dQ^2 dz}(x,Q^2,z) = \frac{d\sigma_{ev}}{dx dQ^2}(x,Q^2) \cdot D^h(x,z,Q^2) . \tag{18}$$

Non-factorisation in x and z at fixed Q^2 implies, that the generalized fragmentation function depends on Bjorken-x.

Non-factorisation has been observed in three BEBC experiments [28,31,39] whereas the 15' $\bar{\nu}Ne\text{-}H_2$ collaboration [12] claims factorisation to hold. Fig. 16 from the BEBC $\bar{\nu}D_2$ experiment [39] shows the average value of z for π^- and π^+ vs. x for all W and for two regions of Q^2. $\langle z\rangle$ is seen to depend on x which implies non-factorisation, the x-dependence being stronger at low Q^2 than at high Q^2. If one selects W > 4 GeV and x_F > 0, no x-dependence is observed (not shown).

A quantitative analysis of non-factorisation has been carried out in terms of

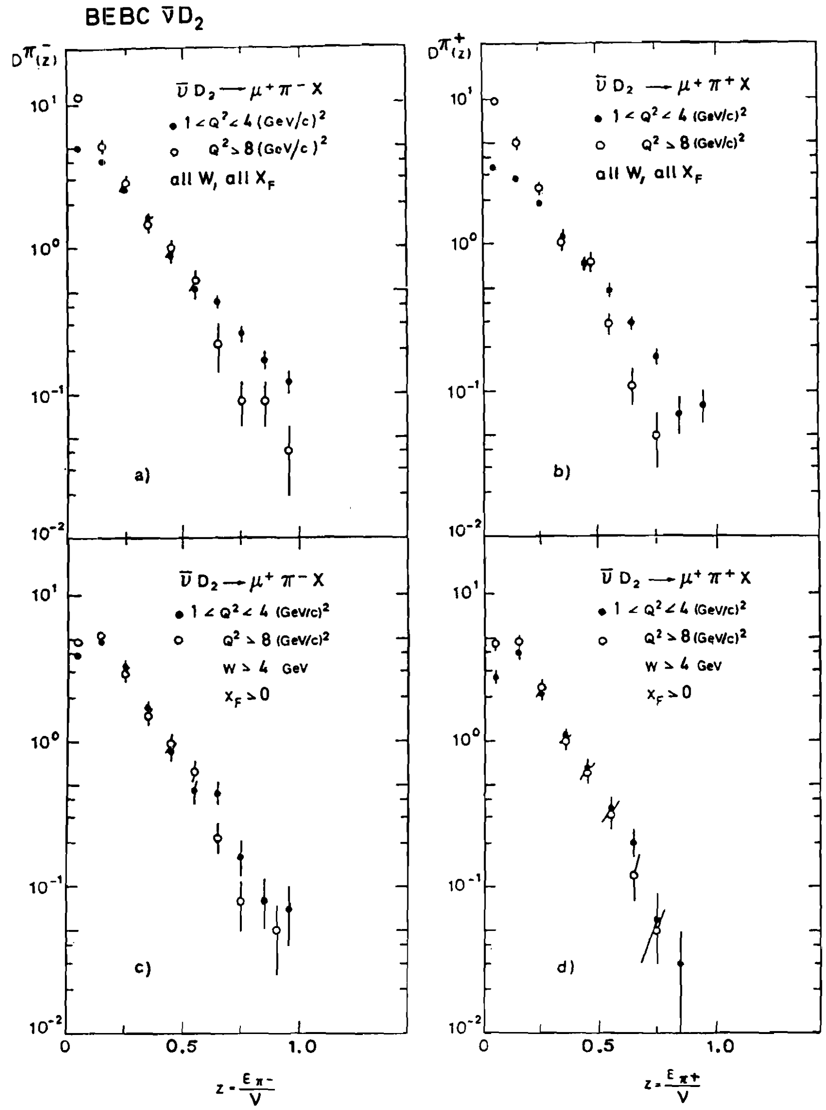

Fig. 15

z-distributions of π^- (a,c) and π^+ (b,d) in $\bar{\nu}N$ scattering for two ranges of Q^2; (a,b) for all W and all x_F, (c,d) for W > 4 GeV and $x_F > 0$, from BEBC $\bar{\nu}D_2$ [39].

double moments [28,31]. In lowest-order QCD, factorisation holds, whereas non-factorisation is predicted [58-60] in next-to-leading order. However, a comparison of the predictions with the measured double moments [28,31] does not show good quantitative agreement between theory and experiment. Only if one includes one further order of QCD [61] a somewhat better agreement is obtained [28].

6.) Higher-twist effects

The contribution of higher twists (HT) to the production of the leading pion (containing the current quark) in lepton-nucleon scattering has been calculated by Berger [62]. The leading pion is a π^+ (containing the u-quark) in νN and a π^- (containing the d-quark) in $\bar{\nu}N$ scattering. Berger derives the following formulae for the differential cross section in $y = \nu/E_\nu$ and z (= energy fraction of the leading pion) for large z and $p_T^2 \ll Q^2$, where p_T is the transverse momentum of the leading pion:

(19a) For $\nu N \to \mu^-\pi^+X$: $d\sigma/dydz \propto (1-z)^2 + \frac{4}{9}(1-y)\cdot\langle k_T^2\rangle/Q^2$,

(19b) For $\bar{\nu}N \to \mu^+\pi^-X$: $d\sigma/dydz \propto (1-z)^2\cdot(1-y)^2 + \frac{4}{9}(1-y)\cdot\langle k_T^2\rangle/Q^2$.

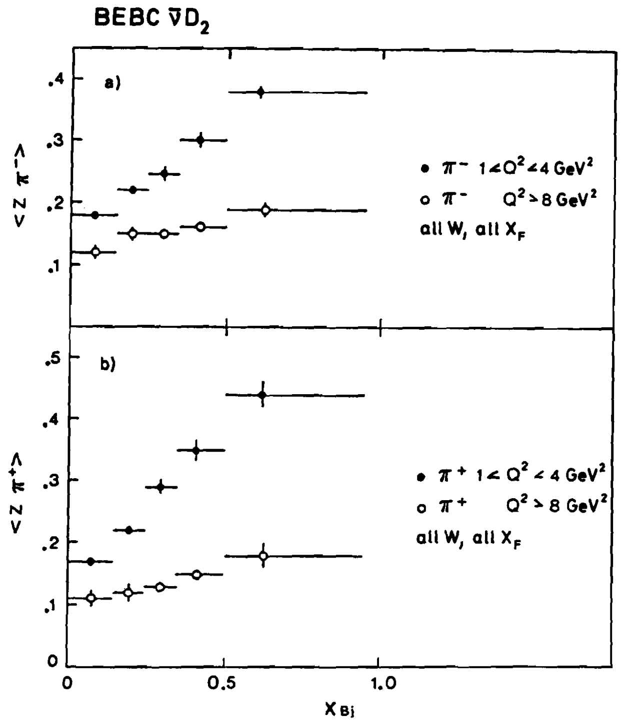

Fig. 16

Average value of z for (a) π^- and (b) π^+ vs. Bjorken-x for two ranges of Q^2 and for all W and all x_F in $\bar{\nu}N$ scattering, from BEBC $\bar{\nu}D_2$ [39].

The second term in each formula is the HT contribution, the relative importance of which increases with decreasing Q^2 and increasing z. The parameter $<k_T^2>$ arises from integrating the original formulae over p_T, but includes also mass terms which were omitted in those formulae. In any case it is a measure for the strength of the HT contribution.

It follows from equ. (19) that due to higher twists one expects a y-z correlation, i.e. non-factorisation in y and z. More specifically:

a) For large z and small Q^2, the y-distribution is expected to behave like (1-y) and thus to deviate from the normal behaviour, which is constant for νN and $(1-y)^2$ for $\bar{\nu}N$.

b) For νN scattering the high-z part of the π^+ z-distribution should fall more steeply (i.e. be softer) for high y than for low y. For $\bar{\nu}N$ scattering on the other hand, the high-z part of the π^- z-distribution should fall less steeply (i.e. be harder) for high y than for low y, due to the extra factor $(1-y)^2$ in the first term.

Mazzanti et al. [63] have pointed out that a y-z correlation is expected also from longitudinal phase space (LPS): For both cases νN and $\bar{\nu}N$, the z-distribution of secondary pions is expected to fall more steeply for high y than for low y. Qualitatively their argument goes as follows: High y means large W, see equ. (2a); at larger W the multiplicity is larger, so that the energy fraction z carried by a single secondary hadron gets smaller which leads to a softer z-distribution. Comparing this with the HT prediction above, one sees that for νN scattering the LPS and HT effects go in the same direction so that a distinction is probably difficult, whereas in case of $\bar{\nu}N$ scattering both effects are opposite to each other so that they may be distinguished from each other (or cancel each other). It should be mentioned however, that the LPS prediction of Mazzanti et al. has been questioned by Berger [64] since it would imply that Feynman-scaling (i.e. energy independence of the z or x_F distribution) is violated already by LPS.

We now discuss the present experimental situation on higher twists. A y-z correlation in the direction as predicted by HT was first observed in νN scattering at low Q^2 by the Gargamelle collaboration [42]. For the parameter $<k_T^2>$ they obtained a value of $<k_T^2> = 1.5 \pm 0.4$ GeV^2. More recently HT effects have been searched for by the 15' $\bar{\nu}Ne\text{-}H_2$ [17], BEBC $\nu,\bar{\nu}Ne\text{-}H_2$ [28], BEBC $\bar{\nu},\nu D_2$ [39], BEBC ν, $\bar{\nu}H_2$ [38] and BEBC $\bar{\nu}Ne\text{-}H_2$ [41] collaborations. We first discuss the case of νN scattering. Fig. 17 shows three examples of π^+ z-distributions $D^{\pi^+}(z)$ at low Q^2 for low and high y. In Fig. 17a from ref. [39] one may notice a small y-z correlation as predicted by HT and LPS, i.e. the z-distribution being softer for high y than for low y. A similar effect is observed in Fig. 17b from ref. [38], where the partially integrated distribution $\int_{z_m}^{1} D(z)dz$ is plotted vs. z_m. On the other hand, no y dependence of the z-distribution is seen in Fig. 17c from ref. [28] which may be explained by the fact that in this experiment a narrow-band beam is used: This beam is more energetic than a usual wide-band beam and therefore yields

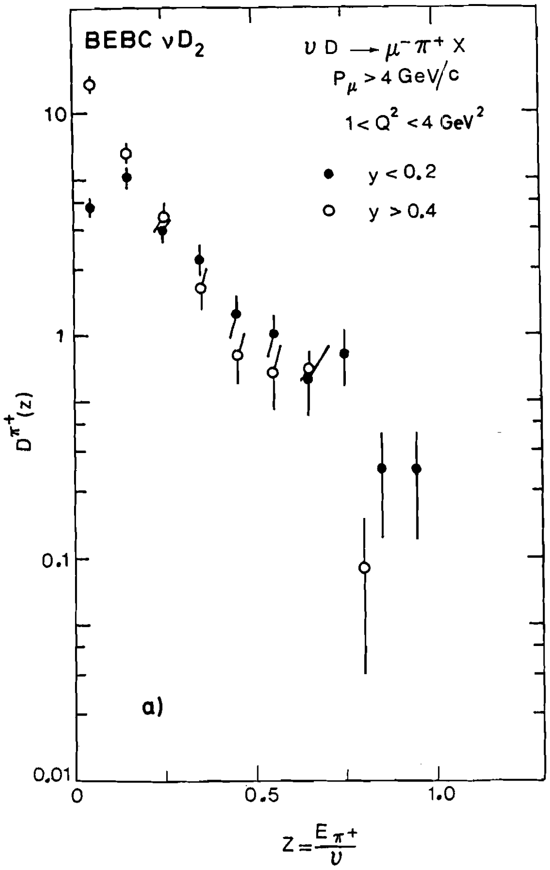

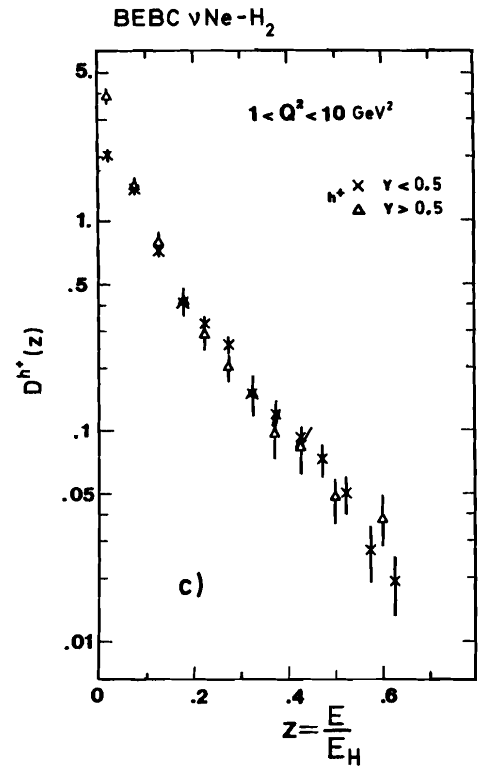

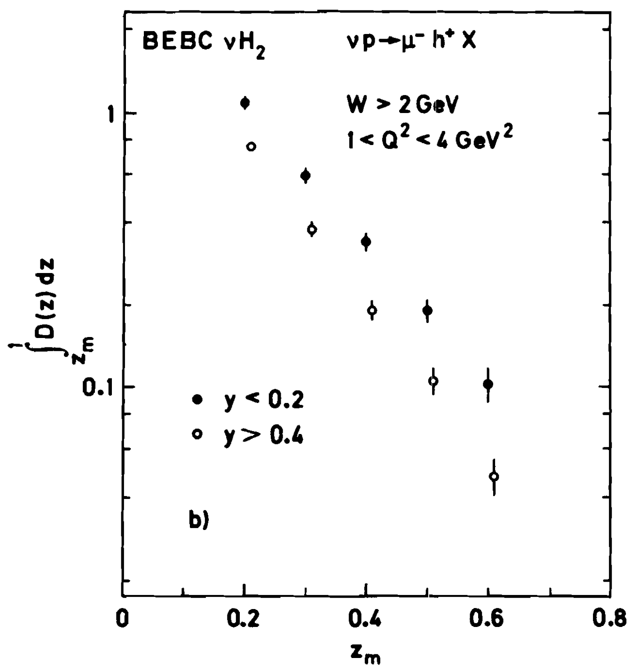

Fig. 17

z-distributions of positive hadrons (mainly π^+) for low and high y in νN scattering at low Q^2, (a) from BEBC $\bar{\nu}, \nu D_2$ [39], (b) from BEBC $\nu, \bar{\nu}H_2$ [38] (preliminary, shown is the partially integrated distribution $\int_{z_m}^{1} D(z)dz$ vs. z_m for W > 2 GeV), (c) BEBC $\nu, \bar{\nu}$Ne-H_2 [28].

only a small fraction of events with lower W. Thus, if the y-z correlation is a low-W effect, it is not expected to show up clearly in this experiment. It should be mentioned that the π^+ distributions of Fig. 17 are contaminated by unidentified protons which may disturb or simulate a y-z correlation for π^+.

We now turn to the case of $\bar{\nu}N$ scattering which is more interesting since the π^- z-distribution is much less contaminated by other unidentified particles and since here HT and LPS make opposite predictions as explained above. Fig. 18 shows three examples of π^- z-distributions $D^{\pi^-}(z)$ at low Q^2 for low and high y. In Fig. 18a from ref. [39] the z-distribution seems to be slightly softer at high y than at low y. This is in the direction as predicted by LPS and opposite to the one predicted by HT. The opposite y-dependence, i.e. a somewhat harder z-distribution at high y and therefore a qualitative agreement with HT is claimed by the 15' $\bar{\nu}Ne$-H_2 collaboration [17] in their π^- z-distribution (Fig. 18b). However the effect is small and the errors on the data points at larger z are relatively large. Finally, the partially integrated z-distributions in Fig. 18c from ref. [38] hardly show any y-dependence which could indicate a cancellation of the LPS and HT effects.

Thus the question of higher-twist effects, in particular in $\bar{\nu}N$ scattering, is not yet solved at present and the situation is unclear. It is worth pointing out however, that inspite of the different conclusions the various data in Fig. 18 are not at all in real disagreement, since different cuts have been applied and since furthermore the observed effects are very small or even doubtful and the experimental errors are large.

In addition to the HT-LPS "interference" a further complication arises: At large y, i.e. small x (see equ. (2c)) the scattering on a sea quark cannot be neglected. Thus in $\bar{\nu}N$ scattering, the reaction

(20a) $\quad \bar{\nu}\bar{d} \rightarrow \mu^+\bar{u}$, $\quad \bar{u} \hookrightarrow \pi^-$

contributes in addition to the normal process

(20b) $\quad \bar{\nu}u \rightarrow \mu^+ d$, $\quad d \hookrightarrow \pi^-$.

The two processes have an opposite y-dependence of the π^- z-distribution, since for reaction (20a) equ.(19a) applies. Therefore a cancellation may occur.

A careful search for higher twists has been performed by the BEBC $\bar{\nu}Ne$-H_2 collaboration [41]. Their analysis includes only events with larger W (in order to reduce the LPS effect) and with $x > 0.15$ (in order to eliminate the scattering on sea quarks). For the π^- z-distribution they find a small additional term as in equ. (19b) which falls with increasing Q^2, which however does not have the predicted y and p_T^2 dependence. Fitting the coefficient $\langle k_T^2 \rangle$ in equ. (19b) they obtain a rather small value of ~ 0.09 GeV^2, much smaller than the Gargamelle value given above. They conclude that there is no evidence for the predicted HT term.

E.) Transverse momentum and jet properties

As usual in leptoproduction, the transverse momentum $\vec{p}_T$ of a secondary hadron is measured perpendicular to the incident-current direction $\hat{q}$ (Fig. 19), which is identical to the direction of the system of all secondary hadrons in the lab frame. For larger W this direction is well approximated by the direction $\hat{q}_H$ of the system of all charged (or visible) hadrons. $\vec{p}_T$ can be decomposed (Fig. 19) into a well measurable component p_n normal to the lepton (ν-μ) plane, which is well defined, and a component in the lepton plane. This latter component is not so precisely measurable since the current direction in the lepton plane is not so well defined due to the uncertainty in estimating the unmeasured neutrino energy of an event. For an isotropic particle distribution around the current direction one expects

(21) $\quad \langle p_n^2 \rangle = \frac{1}{2} \cdot \langle p_T^2 \rangle$.

There are three sources which can contribute to the transverse momentum p_T of a secondary hadron (Fig. 20):

- Fragmentation of partons into hadrons. In the normal case of the simple QPM (Figs. 1,20a) where the final-state partons (quark, diquark) have no transverse

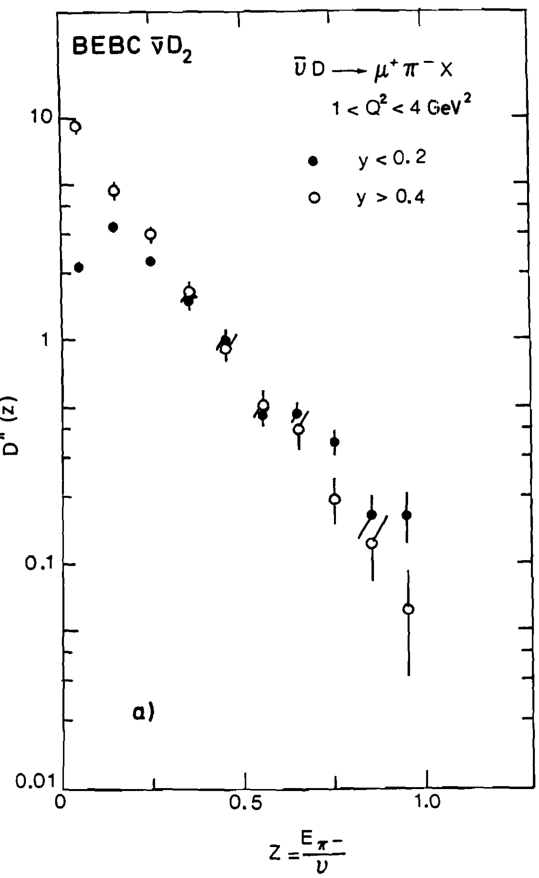

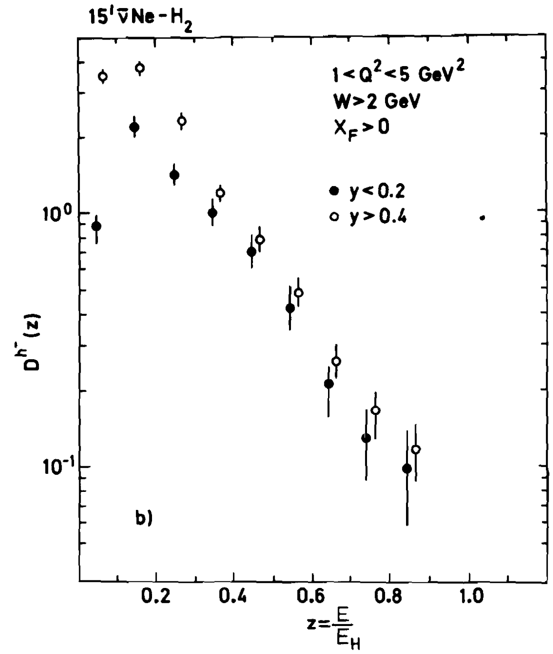

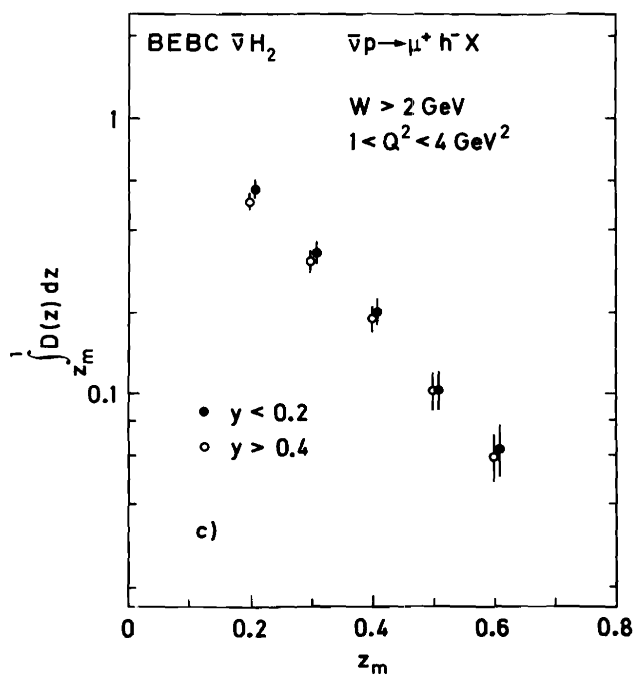

Fig. 18

z-distributions of negative hadrons (π^-) for low and high y in $\bar{\nu}N$ scattering at low Q^2, (a) from BEBC $\bar{\nu}D_2$ [39], (b) from 15' $\bar{\nu}$Ne-H_2 [17] (for W > 2 GeV and $x_F > 0$), (c) from BEBC $\nu,\bar{\nu}H_2$ [38] (preliminary, shown is the partially integrated distribution $\int_{z_m}^{1} D(z)dz$ vs. z_m for W > 2 GeV).

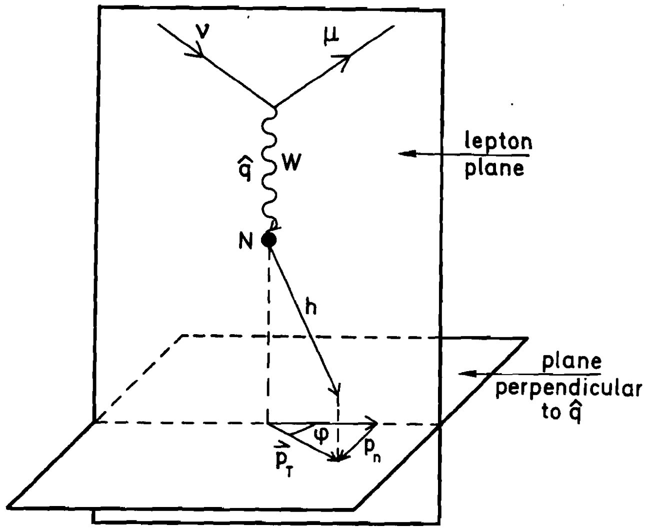

Fig. 19

Definition of the transverse momentum $\vec{p}_T$ of a secondary hadron h.

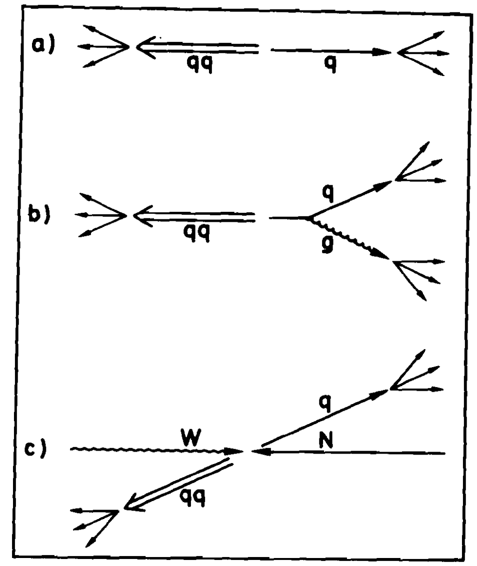

Fig. 20

Processes leading to a transverse momentum of a secondary hadron: (a) fragmentation only, (b) gluon emission by the current quark, (c) primordial transverse momentum.

momentum, the fragmentation is the only source of p_T.

- At higher W, hard QCD processes should show up in some events, for instance the emission of a hard gluon by the current quark after the absorption of the current (Fig. 20b). Here already the forward-going final-state partons (quark, gluon) have a transverse momentum which contributes to the p_T of their hadronic fragments. The diquark on the other hand has no p_T. One thus expects with increasing W a broadening of the p_T distribution in forward direction whereas the p_T distribution of the backward-going diquark fragments should not change with W. In other words, at higher W the jet of forward hadrons is expected to be wider than the backward jet. This expectation remains unchanged qualitatively if the other QCD processes (hard-gluon emission before the absorption of the current, $q\bar{q}$-pair production from a gluon in the nucleon) are also taken into account [65]. Furthermore, at sufficiently high W, some events should show a planar structure (quark-gluon-diquark plane, see Fig. 20b) and, at even higher W, three separate hadronic jets (quark, gluon, diquark) should become discernable in the event plane.
- Primordial transverse momentum k_T of the partons inside the incident nucleon. This k_T is transferred to the final-state quark and diquark such that the event axis (e.g. sphericity axis) has an angle with respect to the current direction (Fig. 20c). Thus the hadronic p_T distributions in the forward and backward hemispheres are broadened, independently of W.

We now confront some recent results from the various experiments with these expectations:

1.) Transverse momentum

Transverse-momentum distributions have been measured for charged hadrons [3,23,35,44,66], π^o[43], strange particles [10,34] and ρ^o mesons [1,26,37]. As an example Fig. 21 shows the p_T^2 distribution of forward-going ($x_F > 0$) charged hadrons for two W intervals from the BEBC νH_2 experiment [35]. At low p_T ($p_T \lesssim$ 1 GeV/c) the distribution is well described by an exponential $e^{-\alpha m_T}$ where $m_T = \sqrt{p_T^2 + m_\pi^2}$ is the transverse mass and $\alpha \approx 6\ \text{GeV}^{-1}$. At higher p_T however there is a tail which becomes more pronounced with increasing W, thus widening the p_T^2 distribution. The curve in Fig. 21 shows a fit $Ae^{-\alpha m_T} + Be^{-\beta m_T}$ with $A = 22.13$ GeV^{-2}, $B = 0.10$ GeV^{-2}, $\alpha = 6.02$ GeV^{-1} and $\beta = 2.07$ GeV^{-1} for $W^2 > 50$ GeV^2.

The widening of the p_T^2 distribution in forward direction ($z > 0.2$) with increasing W is also seen in Fig. 22 of the 15' νNe-H$_2$ collaboration [20,66]. The full curves are QCD predictions [66] for $p_T > 1$ GeV/c; they are in good agreement with the data points.

In Fig. 23, which is a compilation from various experiments [14,23,27,33], the full symbols show the average transverse momentum squared $\langle p_T^2 \rangle$ for forward ($x_F > 0$) and backward ($x_F < 0$) going charged hadrons as a function of W^2. The experiments are in reasonable agreement with each other. In the forward hemisphere $\langle p_T^2 \rangle$ increases with W, thus implying a broadening of the p_T distribution, whereas in the backward hemisphere $\langle p_T^2 \rangle$ is almost independent of W for $W^2 \gtrsim 20$ GeV^2. The same figure also shows $\langle p_n^2 \rangle$ vs. W^2 in the two hemispheres; it is seen that the relation (21) is well fulfilled.

Results on $\langle p_T^2 \rangle$ or $\langle p_T \rangle$ of charged hadrons as a function of W, with the same conclusions as above, are also presented in refs. [3,9,20,44]. They can however not be included in the compilation of Fig. 23, either because $\langle p_T \rangle$ and not $\langle p_T^2 \rangle$ is plotted or because different cuts in x_F or z are applied (seagull effect, see below) in these papers.

The observed widening of the forward p_T distribution with W and the W independence of the backward p_T distribution is in (qualitative) agreement with the prediction of QCD (see above). However, as has been pointed out in ref. [67], also a

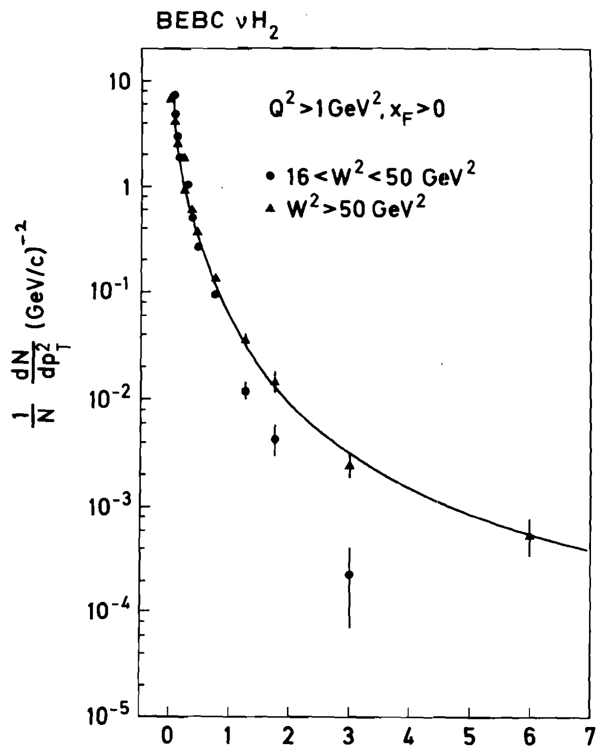

Fig. 21

p_T^2 distribution of forward-going charged hadrons for two W^2 regions in νp scattering, from BEBC νH$_2$ [35]. The curve is a fit of the form $Ae^{-\alpha m_T} + Be^{-\beta m_T}$ to the data points for $W^2 > 50$ GeV^2 (see text) (preliminary).

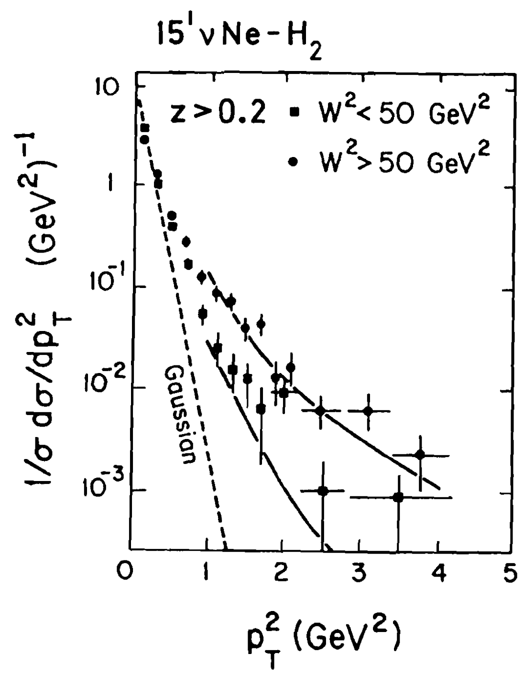

Fig. 22

p_T^2 distribution of charged hadrons with $z > 0.2$ for two W^2 regions in νN scattering, from 15' νNe-H$_2$ [20,66]. The full curves are QCD predictions [66] for $p_T > 1$ GeV/c.

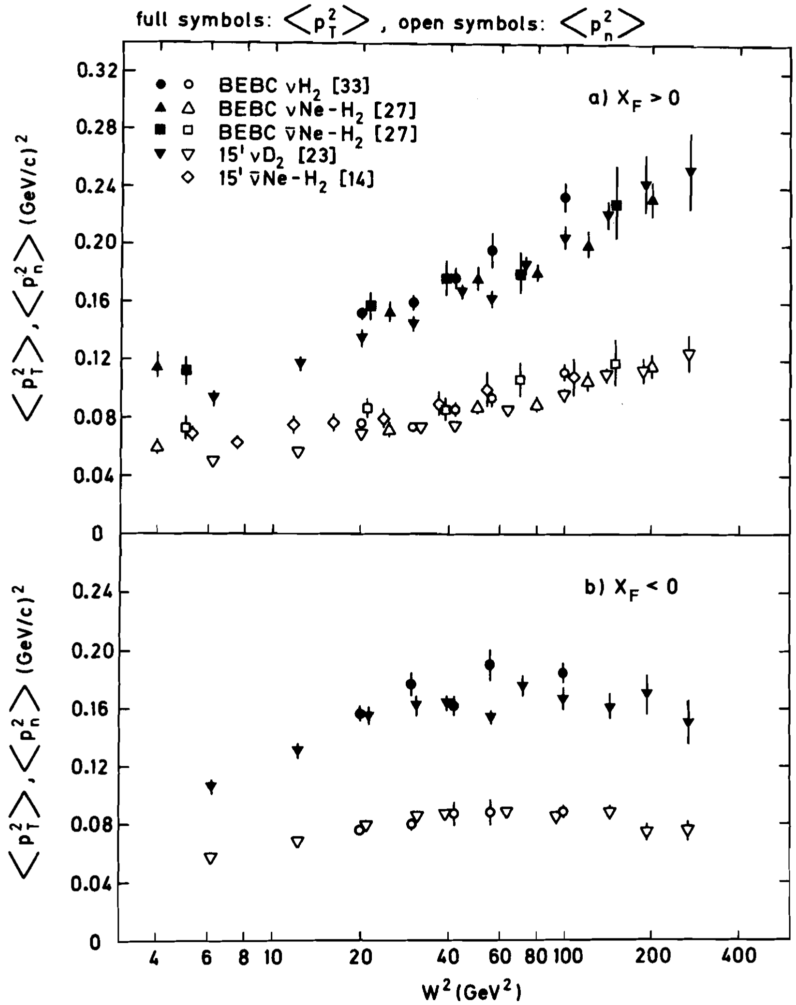

Fig. 23

Compilation of average p_T^2 (full symbols) and average p_n^2 (open symbols) vs. W^2 for (a) forward-going ($x_F > 0$) and (b) backward-going ($x_F < 0$) charged hadrons in νN and $\bar{\nu}N$ scattering from various experiments. p_n is the component of $\vec{p}_T$ normal to the lepton plane.

simple p_T-limited phase space model is able to describe the increase of $\langle p_T \rangle$ with W due to an expansion of available phase space with energy. The observed difference between the forward and backward hemispheres is attributed to the presence of the leading baryon in the backward direction, although no attempt is made in ref. [67] to explain this difference quantitatively.

2.) Seagull effect

The seagull effect, i.e. the rise of $\langle p_T^2 \rangle$ with $|x_F|$ has been investigated in ref. [3,22,27,33,35,43,44]. Fig. 24 shows $\langle p_n^2 \rangle$ vs. x_F for two ranges of W from the BEBC νH_2 experiment [35]. The seagull effect is clearly visible. Furthermore at small W ($4 < W < 6$ GeV) a forward-backward symmetry is observed whereas at large W (> 8 GeV) the seagull effect becomes asymmetric with $\langle p_n^2 \rangle$ being larger in forward than in backward direction at fixed $|x_F|$. The observed asymmetry leads of course directly to the difference, discussed above in connection with Fig. 23, of $\langle p_T^2 \rangle$ in the two hemispheres.

3.) Search for planar events and a three-jet structure

A search for planar events has been carried out by the 15' $\nu Ne-H_2$ [20] and the BEBC νH_2 and $\nu Ne-H_2$ [35] collaborations using almost the same procedure. In both experiments, for each event an event plane is found in the following way: In the plane perpendicular to the direction $\hat{q}$ of the current (or $\hat{q}_H$ of the visible-hadron system) and thus containing $\vec{p}_T$, two orthogonal directions $\hat{u}_{in}$ and $\hat{u}_{out}$ are deter-

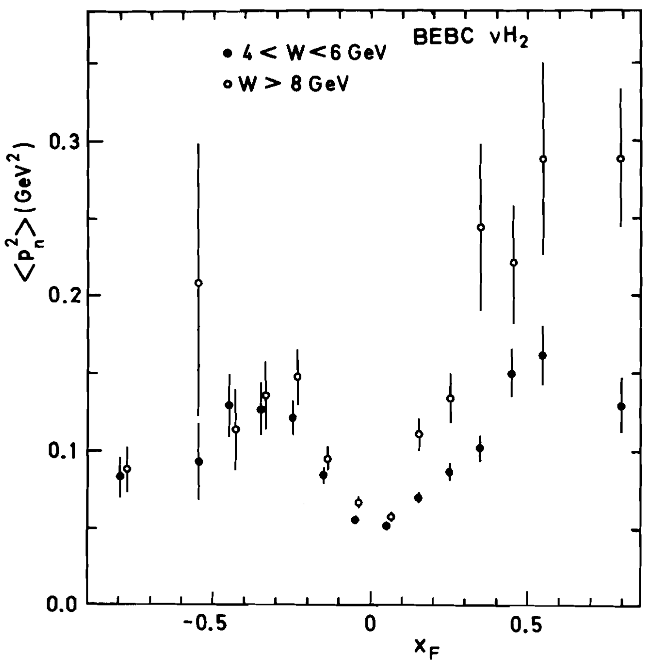

Fig. 24
Average p_n^2 of charged hadrons in νp scattering vs. x_F for two W ranges, from BEBC νH_2 [35] (preliminary). p_n is the component of $\vec{p}_T$ normal to the lepton plane.

mined such that Σp_{Tin}^2 is a maximum and consequently Σp_{Tout}^2 is a minimum. Here p_{Tin} and p_{Tout} are the components of $\vec{p}_T$ along $\hat{u}_{in}$ and $\hat{u}_{out}$, respectively. The sum Σ extends over all visible secondary hadrons in the event. (In ref. [20] tracks with $x_F < -0.7$ are removed since they are predominantly neon fragments). The plane defined by $\hat{q}$ and $\hat{u}_{in}$ is the event plane and the direction $\hat{u}_{out}$ is its normal. A planarity P is then calculated for each event defined by

$$(22) \qquad P = \frac{\Sigma p_{Tin}^2 - \Sigma p_{Tout}^2}{\Sigma p_{Tin}^2 + \Sigma p_{Tout}^2} \; .$$

Furthermore, in ref. [20] a transverse-momentum dispersion

$$(23) \qquad D = \frac{A}{\sqrt{n_F}} \tilde{\Sigma}(p_T - \langle p_T \rangle)$$

is calculated for each event where n_F is the number of forward-going charged hadrons with $x_F > 0.05$ and the sum $\tilde{\Sigma}$ is taken over those hadrons. The factor $1/\sqrt{n_F}$ makes the distribution of D approximately independent of multiplicity. $\langle p_T \rangle$ is set at 0.32 GeV/c, a typical average value for a hadron in a quark jet. The average $\langle D \rangle$ of D is roughly zero and the constant A is chosen such that $\langle D^2 \rangle = 1$. An event with a large value of D contains one or more forward hadrons with large p_T, D thus being a measure of how strongly the particles are spread out in transverse momentum.

Fig. 25 of ref. [20] shows a scatter plot of planarity P vs. dispersion D for 1552 events with $W^2 > 50$ GeV^2 and $Q^2 > 2$ GeV^2. It is seen that events with a high D have a tendency to be more planar than normal events: For $D > 3.0$ (55 events, i.e. ~4% of all events) $\langle P \rangle = 0.73 \pm 0.02$, whereas for $D < 2.0$ $\langle P \rangle = 0.51 \pm 0.01$. This occurrence of a small fraction of planar events could be due to hard-gluon emission as discussed above. It could however also be the tail of a normal longitudinal phase space distribution and thus a purely kinematical effect: The high p_T in an event with large D has to be balanced, and since only a limited amount of energy is available, the balancing particles tend to lie opposite to the high-p_T particle, thus making the event flat. Nevertheless, assuming forward-backward symmetry for the normal two-jet component it is shown in ref. [20] that out of the 55 events with $D > 3.0$ only 14 ± 4 events are background from a phase-space tail, leaving a net signal of 41 ± 9 events possibly due to hard-gluon emission.

A very similar result has been obtained by the BEBC νH_2 and BEBC νNe-H_2 collaborations [35]. Here the constant in equ. (23) is set to $A = 1$, the sum $\tilde{\Sigma}$ is taken over all forward-going charged hadrons in an event and $\langle p_T \rangle$ is the averaged transverse momentum of forward hadrons in all events. Fig. 26 shows the planarity distribution for events with $n_F \geq 3$, $W > 4$ GeV and $Q^2 > 1$ GeV^2, (a) without selection on D and (b) for events with a D exceeding $\langle D \rangle$ (≈ 0) by more than two standard deviations σ of the D distribution, i.e. with $D > \langle D \rangle + 2\sigma$. The event sample (b) constitutes ~3% of sample (a) and consists of events with large W ($\gtrsim$ 8 GeV). Again it is seen that events with large D tend to be more planar than normal events.

The 15' νNe-H_2 [20] and BEBC νH_2 [35] collaborations have both measured the

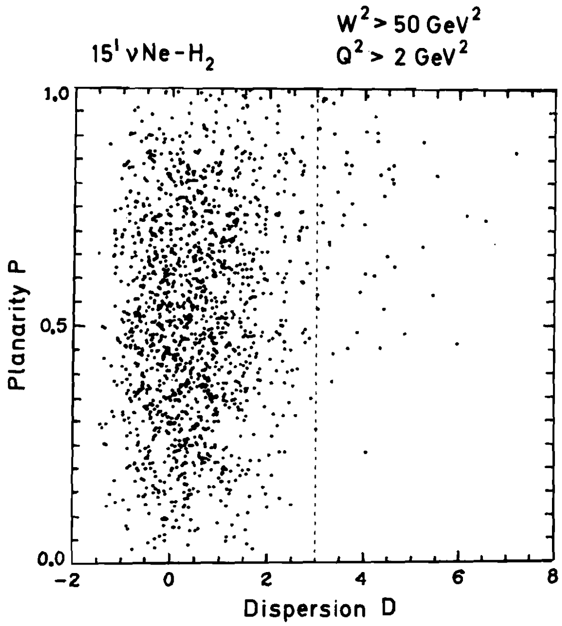

Fig. 25

Scatter plot of planarity P (equ.(22)) vs. transverse-momentum dispersion D (equ. (23)) for νN events with $W^2 > 50\ GeV^2$ and $Q^2 > 2\ GeV^2$, from 15' νNe-H_2 [20].

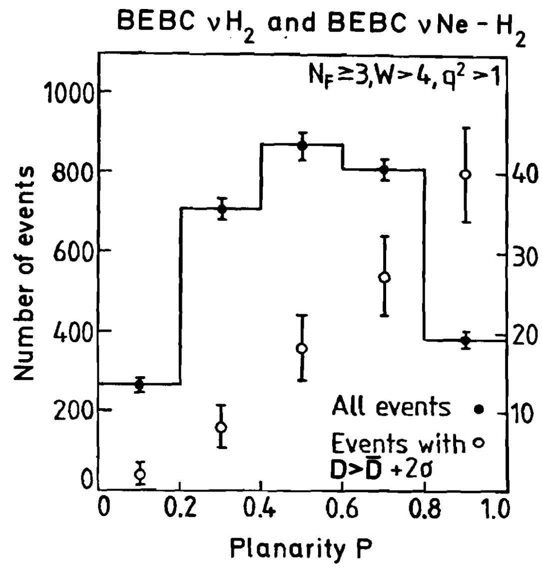

Fig. 26

Distribution of Planarity P (equ.(22)) for νN events with $n_F \geqslant 3$, $W > 4$ GeV and $Q^2 > 1\ GeV^2$. The histogram (full points) is for all events (scale on left hand side), the open circles are for events with $D > \langle D\rangle + 2\sigma$ (see text) (scale on right hand side). From BEBC νH_2 and BEBC νNe-H_2 [35] (preliminary).

angular energy flow which is defined by

$$\frac{d\varepsilon}{d\Theta} = \frac{1}{N_{ev}} \frac{\Sigma z_i}{\Delta\Theta} \ . \tag{24}$$

Here z_i is the cms-energy fraction of a hadron and Θ the angle between the current direction $\hat{q}$ and the projection of the hadron momentum in the event plane $(\hat{q}$-$\hat{u}_{in})$ or in the plane $(\hat{q}$-$\hat{u}_{out})$ perpendicular to the event plane, respectively. The sum extends over all charged hadrons in the angular interval between Θ and $\Theta + \Delta\Theta$.

Fig. 27 shows the angular energy flow in the event plane from the 15' νNe-H_2 experiment [20], (a) for all events with $W^2 > 50\ GeV^2$ and (b) for the small subsample of events with $D > 3.0$ and $P > 0.5$. The bulk of events has the usual two-jet structure as expected from the simple QPM (Fig. 20a). The subsample (b) of planar events however shows a broadening of the energy flow in the forward hemisphere with a pronounced dip in the forward direction. This implies a three-jet structure (two forward jets, one backward jet) in the event plane as expected from hard-gluon emission (Fig. 20b). The dip in the middle could again be a consequence of p_T balance, but as mentioned above, the authors claim that phase space can account only for part of the effect.

The angular energy flow as measured by the BEBC νH_2 collaboration [35] in the event plane and in the perpendicular plane is shown in Fig. 28 for events with $W > 4$ GeV, $Q^2 > 1\ GeV^2$ and with at least one forward particle having a $p_T > 1$ GeV/c. Again, in the event plane a dip in forward direction is observed implying a two-jet structure in the forward hemisphere, whereas in the perpendicular plane the energy is accumulated, as expected, in the forward and backward direction. There is little difference between the two orthogonal planes in the backward (diquark) direction.

Finally Fig. 29 of the BEBC νH_2 and νNe-H_2 collaborations [35] shows for

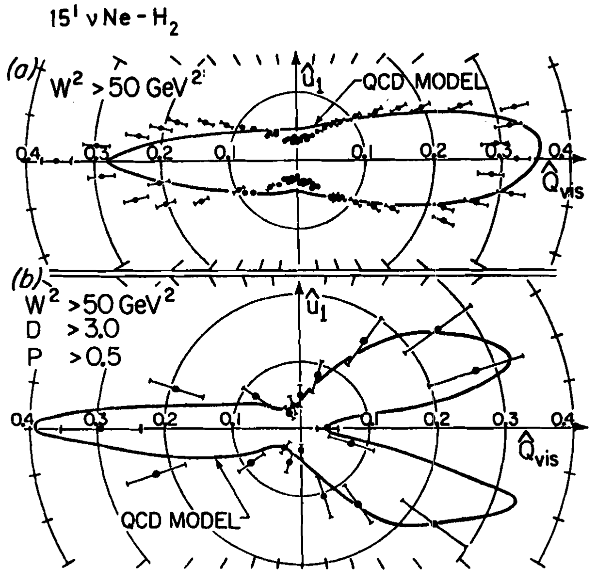

Fig. 27

Angular energy flow (equ.(24)) in the event plane in νN scattering, (a) for all events with $W^2 > 50$ GeV^2 and (b) for events with $W^2 > 50$ GeV^2, dispersion $D > 3$ and planarity $P > 0.5$, from 15' νNe-H_2 [20]. The curves are predictions of a QCD model.

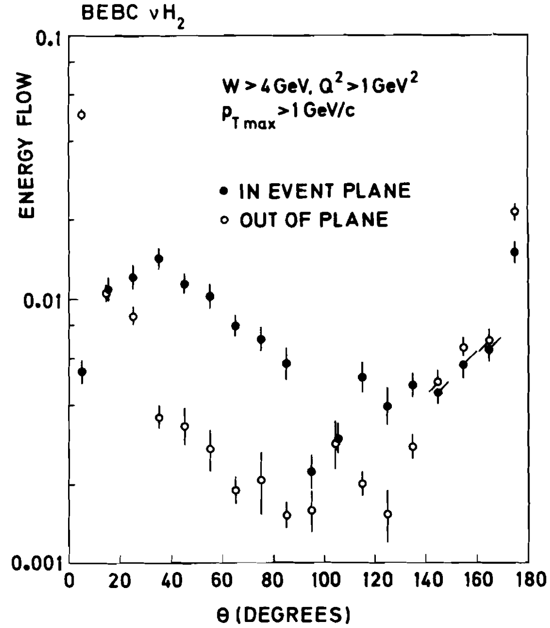

Fig. 28

Angular energy flow in the event plane (full points) and in the plane perpendicular to the event plane (open circles) for νp events with $W > 4$ GeV, $Q^2 > 1$ GeV/c and $p_{Tmax} > 1$ GeV/c, from BEBC νH_2 [35] (preliminary). p_{Tmax} is the highest transverse momentum of a forward-going charged hadron in the event.

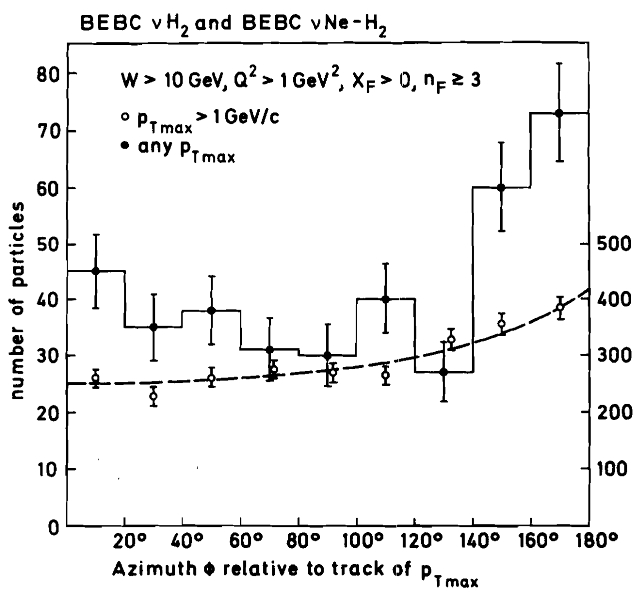

Fig. 29

Azimuthal angular distribution of forward-going charged hadrons in νN events with $W > 10$ GeV, $Q^2 > 1$ GeV^2, $n_F \geqslant 3$. $\phi = 0$ is defined by the hadron with the highest p_T. The open circles are for all events (scale on right hand side), the histogram (full points) is for events with $p_{Tmax} > 1$ GeV/c (scale on left hand side). The dashed curve is an eyeball fit through the open circles. From BEBC νH_2 and BEBC νNe-H_2 [35] (preliminary).

events with $W > 10$ GeV and $Q^2 > 1$ GeV^2 the distribution of the azimuthal angle ϕ around the direction $\hat{q}_H$ of the charged-hadron system (i.e. in the $\hat{u}_{in}$-$\hat{u}_{out}$ plane) for forward-going charged hadrons. The $\phi = 0$ axis is defined by the hadron with the largest p_T, p_{Tmax}. (This hadron is not included in Fig. 29). The ϕ distribution is shown (a) without selection on p_{Tmax} and (b) for events with a $p_{Tmax} > 1$ GeV/c. The distribution for sample (a) is rather isotropic with an excess, due to p_T balance, on the side opposite ($\phi \approx 180^o$) to the highest-p_T hadron. A much stronger excess of hadrons with ϕ near 180^o is seen for sample (b). In this sample there might be in addition some accumulation of hadrons at small ϕ, thus travelling with the p_{Tmax} particle and therefore contributing to the flatness of the event. This accumulation, if it exists, cannot be explained by p_T balance. It could be due to production of heavy resonances or again indicate a two-jet structure in the forward hemisphere.

It should be mentioned that a broadening of the p_T distribution in forward direction with increasing W, the occurrence of planar events with a three-jet structure, and an unisotropic ϕ distribution with accumulations around $\phi = 0^o$ and 180^o has also been observed in muoproduction by the European Muon Collaboration [68] at higher values of W ($W > 10$ GeV).

4.) Azimuthal unisotropy

As mentioned above (Fig. 20b,c), the forward-going current quark can acquire a transverse momentum with respect to the current direction due to QCD processes and/or the primordial k_T. This transverse momentum is not isotropically distributed around the current direction, but has an azimuthal angular distribution of the form [69,70]

$$\frac{d\sigma}{d\varphi} = A + B\cdot\cos\varphi + C\cdot\cos 2\varphi \qquad (25)$$

where $\varphi = 0$ in the lepton plane towards the muon (see Fig. 19). For the average values QCD [69] predicts the following Q^2 dependences:

$$\langle\cos\varphi\rangle \propto -1/\ln\frac{Q^2}{\Lambda^2} \quad \text{and} \quad \langle\cos 2\varphi\rangle \propto 1/\ln\frac{Q^2}{\Lambda^2} \qquad (26)$$

where Λ is the QCD parameter in the running coupling constant. In the presence of a primordial k_T on the other hand, the Q^2 dependences are expected [70] to be as follows:

$$\langle\cos\varphi\rangle \propto -\langle k_T\rangle/\sqrt{Q^2} \quad \text{and} \quad \langle\cos 2\varphi\rangle \propto \langle k_T^2\rangle/Q^2. \qquad (27)$$

Both effects predict the same signs and should in principle be distinguishable from each other by their different Q^2 behaviour, provided that sufficiently accurate data are available. Of course an unisotropy of the current-quark distribution leads to an unisotropy of its hadronic fragments, although smeared out by the fragmentation process.

Recent investigations on the φ distributions have been carried out by the 15' $\bar{\nu}H_2$ [3] and 15' $\bar{\nu}$Ne-H_2 [18] collaborations. No statistically significant unisotropy is seen in ref. [3]. Fig. 30 shows $\langle\cos\varphi\rangle$ and $\langle\cos 2\varphi\rangle$ vs. Q^2 for forward-going negative hadrons with $z > 0.2$ from ref. [18]. The average value $\langle\cos\varphi\rangle$ seems to deviate from zero with the predicted minus sign. However, the errors on both averages are large so that no distinction between the two effects (26) and (27) is possible. For the whole Q^2 range the following values are obtained:

$$\langle\cos\varphi\rangle = -(0.156 \pm 0.054) \quad \text{and} \quad \langle\cos 2\varphi\rangle = 0.031 \pm 0.027$$

after correcting for unseen neutrals and intranuclear cascades in the Ne nuclei.

5.) Primordial transverse momentum k_T

As mentioned above (Fig. 20c) a primordial k_T of the interacting quark inside the incident nucleon leads to an angle between the event axis (e.g. sphericity axis or direction of the charged-hadron system) and the current direction. Measuring this angle and estimating the momentum of the fragmenting quark from the momenta of its hadronic fragments, the following estimates have been obtained by the BEBC νH_2 collaboration [33]:

$$\langle k_T^2\rangle \approx 0.3\,(\text{GeV/c})^2 \quad \text{and} \quad \langle k_T\rangle \approx 0.55 \text{ GeV/c}.$$

A somewhat different method has been applied by the 15' $\bar{\nu}$Ne-H_2 collaboration [14]. They determine the average transverse momentum squared with respect to the

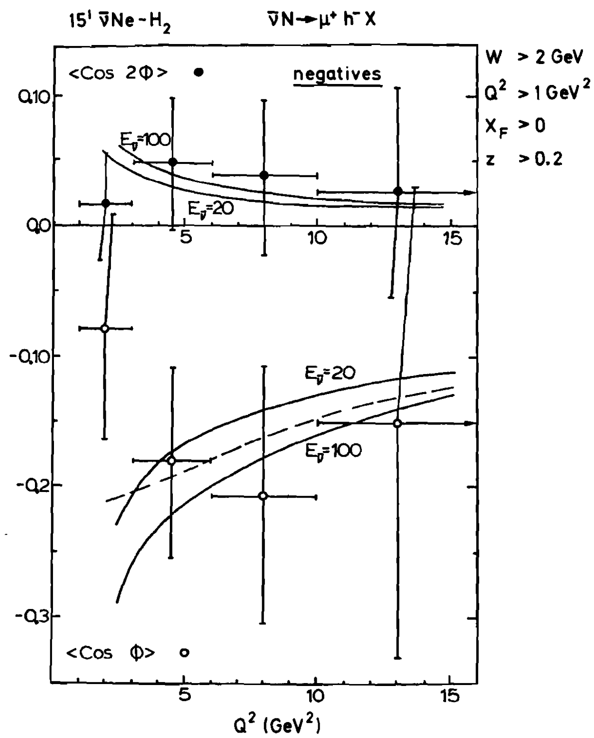

Fig. 30

Average values $\langle\cos\varphi\rangle$ (open circles) and $\langle\cos 2\varphi\rangle$ (full points) for forward-going ($x_F > 0$) negative hadrons with $z > 0.2$ in $\bar{\nu}$N events with $W > 2$ GeV, $Q^2 > 1$ GeV^2, from 15'$\bar{\nu}$Ne-H$_2$ [18]. The full curves are QCD predictions for $E_{\bar{\nu}} = 20$ and 100 GeV. The dashed curve is a prediction of the QPM with primordial $\langle k_T\rangle = 0.8$ GeV/c and $\langle p_T\rangle_{fragm.} = 0.36$ GeV/c.

thrust axis and identify this with the contribution $\langle p_T^2\rangle_{fragm.}$ from fragmentation alone. Subtracting $\langle p_T^2\rangle_{fragm.}$ from $\langle p_T^2\rangle$ (with respect to the current direction) and neglecting the QCD contribution one obtains $\langle z^2\rangle\langle k_T^2\rangle$, i.e. the contribution of k_T to the $\langle p_T^2\rangle$ of the current fragments. Using the measurement $\langle z^2\rangle = 0.14 \pm 0.01$, a value of

$$\langle k_T^2\rangle = (0.4 \pm 0.1)(\text{GeV/c})^2$$

is obtained for the primordial k_T.

F.) Conclusions

Without repeating the details one may summarize the present situation as follows:

1.) Many new and more precise data on hadron production in νN and $\bar{\nu}$N scattering have been gained during the last year. In particular, for the first time good results are now available on ν and $\bar{\nu}$ scattering on neutrons.

2.) The quark-parton model works successfully and is able to explain the main features of νN and $\bar{\nu}$N scattering.

3.) Multiplicities: Here many similarities between νN/$\bar{\nu}$N scattering and non-diffractive hadron-hadron scattering are observed.

4.) Fragmentation functions:
- In addition to the fragmentation functions of quarks also those of diquarks have been measured now. The main properties of fragmentation functions are in agreement with the QPM.
- The observed violation of scaling and factorisation is not yet really well understood theoretically, in particular not yet in the case of $\bar{\nu}$N scattering.
- The situation on higher twists is still unclear; the contributions from higher twists seem to be small. More accurate data at high z and more detailed analyses are needed.

5.) Transverse momentum and jet properties:
- The QCD-predicted broadening of the p_T distribution in the forward hemisphere is clearly seen.
- There are indications that a small subsample of events are planar and might even have a three-jet structure, beyond simple p_T balance.

6.) Higher neutrino energies are highly desirable so that the kinematical overlap of current and target fragments can be further reduced and hard QCD processes show up more clearly.

I would like to thank my colleagues in the various collaborations for many enlightening and fruitful discussions. I express my gratitude to Mrs. A. Harnisch for drawing a major part of the figures and to my secretary Mrs. E. Thurner for her careful and diligent work in typing the manuscript and in arranging the figures in the text. Finally I thank my friends at Bonn University for their hospitality and manifold help during the Bonn conference.

References

1.) M. Derrick et al.: Phys. Lett. 91B (1980) 307
2.) M. Derrick et al.: Phys. Lett. 91B (1980) 470
3.) M. Derrick et al.: Phys. Rev. D24 (1981) 1071
4.) M. Derrick et al.: Multiplicity distributions in $\bar{\nu}_\mu p$ interactions, Preprint ANL-HEP-PR-81-01 (1981)
5.) R. Brock et al.: Strange particle production in high energy $\bar{\nu}$ and ν charged current interactions on protons, Preprint ANL-HEP-PR-81-24 (1981)
6.) J.P. Berge et al.: Phys. Rev. D22 (1980) 1043
7.) J.P. Berge et al.: Phys. Lett. 91B (1980) 311
8.) V.V. Ammosov et al.: Phys. Lett. 93B (1980) 210
9.) V.V. Ammosov et al.: Phys. Lett. 102B (1981) 213
10.) V.V. Ammosov et al.: Nucl. Phys. B162 (1980) 205
11.) V.V. Ammosov et al.: Nucl. Phys. B177 (1981) 365
12.) J.P. Berge et al.: Nucl. Phys. B184 (1981) 13
13.) V.V. Ammosov et al.: Quark jets from antineutrino interactions II; inclusive particle spectra and multiplicities in the quark-jets, FERMILAB-Pub-80/96-Exp (1980); paper No. 233, submitted to this conference
14.) J.P. Berge et al.: Quark jets from antineutrino interactions III; transverse structure of the quark jets, FERMILAB-Pub-81/30-Exp (1981); paper No. 229, submitted to this conference
15.) R. Orava: Charge compensation in the quark jets, FERMILAB-Pub-81/16-Exp(1981)
16.) R. Orava: Quark jets from deeply inelastic lepton scattering, FERMILAB-Conf-81/21-Exp (1981)
17.) V.V. Ammosov et al.: Higher-twist effects in semi-inclusive $\bar{\nu}N\to\mu^+h^\pm X$ reactions, IHEP 81-89 (1981)
18.) V.V. Ammosov et al.: Azimuthal asymmetry of negative hadrons produced in $\bar{\nu}N\to\mu^+h^-X$ reaction, paper No. 184, submitted to this conference
19.) V.V. Ammosov et al.: Search for quark polarization effects in charged-current antineutrino-nucleon interactions, paper No. 186, submitted to this conf.
20.) H.C. Ballagh et al.: Phys. Rev. Lett. 47 (1981) 556; paper No. 194, submitted to this conference
21.) T. Kitagaki et al.: Characteristics of charged particle multiplicity distributions in high energy νn and νp interactions, Contrib. to the XX. Intern. Conf. on High Energy Physics, Madison (1980)
22.) T. Kitagaki et al.: Current and target jets produced in high energy νD interactions, Contrib. to the XX.Intern.Conf. on High Energy Phys., Madison (1980)
23.) T. Kitagaki et al.: Phys. Lett. 97B (1980) 325
24.) D. Zieminska et al.: Production of hadrons in high energy νD interactions, Contrib. to the 12. Intern. Symp. on Multiparticle Dynamics, Notre Dame (1981)
25.) C.C. Chang et al.: Diquark fragmentation into Λ particles in νp and νn interactions, Contrib. to the 12. Intern. Symp. on Multiparticle Dynamics, Notre Dame (1981)
26.) C.C. Chang et al.: Inclusive meson resonance production and fragmentation of u-quark jets in high energy νD interactions, Contrib. to Neutrino 81 Conf., Maui, Hawaii (1981)
27.) H. Deden et al.: Nucl. Phys. B181 (1981) 375
28.) H. Deden et al.: Analysis of fragmentation functions of narrow band ν and $\bar{\nu}$ interactions on an isoscalar target, Aachen-Bonn-CERN-Demokritos-London (I.C.)-Oxford-Saclay Collab., draft (1981)
29.) P. Allen et al.: Phys. Lett. 96B (1980) 209
30.) P. Allen et al.: Nucl. Phys. B176 (1980) 269
31.) P. Allen et al.: Nucl. Phys. B176 (1980) 333
32.) P. Allen et al.: Nucl. Phys. B181 (1981) 385
33.) P. Allen et al.: Nucl. Phys. B188 (1981) 1
34.) H. Grässler et al.: Inclusive neutral strange particle production in νp interactions, CERN/EP 81-56 (June 1981)

35.) Aachen-Bonn-CERN-München(MPI)-Oxford Collab. and Aachen-Bonn-CERN-Demokritos-London-Oxford-Saclay Collab.: Transverse properties of hadrons produced in neutrino-nucleon scattering in BEBC, Contrib. to the Neutrino 81 Conf., Maui, Hawaii (1981); and paper in preparation

36.) Aachen-Bonn-CERN-München(MPI)-Oxford Collab.: Investigation of quark and diquark fragmentation in neutrino-proton charged-current interactions in BEBC, Contrib. to the Neutrino 81 Conf., Maui, Hawaii (1981)

37.) Aachen-Bonn-CERN-München(MPI)-Oxford Collab.: Inclusive production of ρ^o in νp charged current interactions, CERN/EP 81-93 (1981)

38.) Aachen-Bonn-CERN-München(MPI)-Oxford Collab.: private communication from B. Saitta

39.) D. Allasia et al.: Fragmentation functions in high energy $\bar{\nu}D_2$ interactions, paper No. 188, submitted to this conference

40.) S. Barlag et al.: Charged hadron multiplicities in high energy $\bar{\nu}_\mu n$ and $\bar{\nu}_\mu p$ interactions, paper No. 189, submitted to this conference

41.) Bari-Birmingham-Brussels-CERN-Demokritos-Ecole Polytechnique-Imperial College London-Munich-Oxford-Rutherford-Saclay-University College London Collab.: Search for higher twist effects in semi-inclusive deep-inelastic antineutrino scattering, draft

42.) M. Haguenauer et al.: Phys. Lett. 100B (1981) 185

43.) E.P. Kuznetsov et al.: Inclusive γ and π^o production in νN and $\bar{\nu}N$-interactions in the energy range 3-25 GeV/c, paper No. 182; submitted to this conference

44.) E.P. Kuznetsov et al.: Inclusive properties of charged pions in $\bar{\nu}N$-interactions in the energy range 3-25 GeV, paper No. 183; submitted to this conference

45.) B. Saitta : Review talk presented at the Neutrino 80 Conf. Erice, 1980.

46.) N. Schmitz: Proc. Intern. Symp. on Lepton and Photon Interactions at High Energies, Fermilab, p. 359 (1979)

47.) A. Wroblewski : Acta Phys. Polonica B4 (1973) 857

48.) T. Fields et al.: Proc. Liblice-Prague Symp. on Antinucleon-Nucleon Interactions, CERN 74-18, p. 151 (1974)

49.) A. Wroblewski: Contrib. to the 12. Intern. Symp. on Multiparticle Dynamics, Notre Dame, 1981

50.) Z. Koba, H.B. Nielsen, P. Olesen: Nucl. Phys. B40 (1972) 317

51.) A. Wroblewski: Private communication

52.) R.D. Field, R.P. Feynman: Nucl. Phys. B136 (1978) 1

53.) R.D. Field, R.P. Feynman: Phys. Rev. D15 (1977) 2590

54.) L.M. Sehgal: Proc. 1977 Intern. Symp. on Lepton and Photon Interactions at High Energies, Hamburg, p. 837 (1977)

55.) P.C. Bosetti et al.: Nucl. Phys. B149 (1979) 13

56.) V. Blobel et al.: Nucl. Phys. B69 (1974) 454

57.) J. Blietschau et al.: Phys. Lett. 87B (1979) 281

58.) N. Sakai: Phys. Lett. 85B (1979) 67

59.) G. Altarelli et al.: Nucl. Phys. B160 (1979) 301

60.) R. Baier, K. Fey: Z. Phys. C2 (1979) 339

61.) J. Sheiman, I. Hinchliffe, H.E. Haber: Nucl. Phys. B183 (1981) 397

62.) E.L. Berger: Phys. Lett. 89B (1980) 241; Z. Phys. C4 (1980) 289

63.) P. Mazzanti, R. Odorico, V. Roberto: Phys. Lett. 98B (1981) 360

64.) E.L. Berger: Private communication

65.) P.M. Stevenson: Nucl. Phys. B156 (1979) 43
R.D. Peccei, R. Rückl: Nucl. Phys. B182 (1981) 21

66.) M. Dechantsreiter, F. Halzen, D.M. Scott: Z. Phys. C8 (1981) 85

67.) A.B. Clegg, A. Donnachie: Preprint M/C TH 81/11 (1981)

68.) J.J. Aubert et al.: Phys. Lett. 95B (1980) 306; 100B (1981) 433
H.E. Montgomery: Rapporteur's talk at this conference

69.) H. Georgi, H.D. Politzer: Phys. Rev. Lett. 40 (1978) 3
A. Mendez: Nucl. Phys. B145 (1978) 199
A. Mendez, A. Raychaudhuri, V.J. Stenger: Nucl. Phys. B148 (1979) 499

70.) R.N. Cahn: Phys. Lett. 78B (1978) 269

Discussion

K. H. Becks, Gesamthochschule Wuppertal: You observe scale breaking and factorization break-down only if you include all W. Is the resonance region excluded?

N. Schmitz: No, if we take all W then the resonance region is of course included. However, if one makes a rather low W cut, say at about 2 GeV, then also one sees scale breaking and non-factorization.

B. R. Webber, Univ. of Cambridge: I would like to make a comment about jet-broadening in QCD. Both, the quark and diquark jets are predicted to get broader in deep inelastic final states, due to bremsstrahlung of gluons by the struck quark before interaction with the current. This gives a smaller broadening for the diquark jet than the quark jet (which includes the recoiling quark) but it would be interesting to see this effect.

N. Schmitz: Yes, you are right. In the case of bremsstrahlung before the current absorption one has a backward going gluon together with the diquark, leading to a broadening of the p_T in backward direction. But also in this case the forward going current quark has a p_T. So the current quark always gets a p_T independently of what kind of QCD process takes place. The widening of the p_T distribution in the backward hemisphere by QCD processes has been calculated by Peccei and Rückl and turned out to be small as compared to the broadening in the forward hemisphere.

E. L. Berger, Argonne Nat. Lab.: Let me comment briefly on the analyses of higher twist effects. You conclude that the higher twist contributions may be very small, but I don't think that one can conclude that from the way the data have been analyzed. The bulk of the data which you show are in the region of $z \leq .5$ and most of the curves which you show as a function of z stop for $z < .6$ or .7. However, the higher twist effects are predicted to be important at larger z. My predictions are for changes in the y distribution as $z \to 1$; thus, you should select data on the basis of cuts in z and plot them as a function of y (instead of the other way around). The Gargamelle group made such an anlysis a few years ago and evidently was able to extract a higher twist contribution.

N. Schmitz: Let me first point out that, as a rapporteur, I have presented the higher twist analyses of other groups, not mine. Secondly, at large z there are rather few particles and the fragmentation functions go down very steeply. Let me show you the original data of the Gargamelle collaboration; they indeed claim to see an effect. They get for $\langle p_t^2 \rangle$ in the higher twist term about 1.5 GeV^2. But, as I said, if the LPS analysis of Mazzanti et al. is correct, one would expect a similar effect just from phase-space. From antineutrino scattering the $\langle p_t^2 \rangle$ turns out to be much smaller, about 0.07 - 0.09 GeV^2. So, I still think that the situation is more complicated due to the contributions from phase space and antiquarks.

E. L. Berger: If your statement is that there are no data at large z, then your conclusion should be that you have nothing to say about higher twist. Let me add another comment. You make the statement that LPS (phase space) means that as you increase W, the z distribution softens. If that were true, then LPS would be predicting scaling violations and we would not need either logarithmic QCD or higher twist. I don't think that is reasonable. What should be built into the phase space minimal bias program is scaling in the variable z and not some LPS assumptions which clearly disagree with everything we have learnt.

G. Wolf, DESY: I have a question to the diquark fragmentation analyses. Two extreme views for diquarks are

1. the two quarks are in a coherent state,
2. the two quarks are acting incoherently.

In the second case the diquark fragmentation function would just be the sum of the quark fragmentation functions. Is there any evidence for a coherent piece?

N. Schmitz: Such a separation of the break-up contribution and the coherent contribution has not yet been carried out.